Boillot, G., Winterer, E. L., et al., 1988
Proceedings of the Ocean Drilling Program, Scientific Results, Vol. 103

31. RESEDIMENTATION AND DIAGENESIS, INCLUDING SILICIFICATION, OF BARREMIAN-APTIAN SHALLOW-WATER CARBONATES FROM THE GALICIA MARGIN, EASTERN NORTH ATLANTIC, AT OCEAN DRILLING PROGRAM SITE 641[1]

Janet A. Haggerty and Scott H. Germann, Department of Geosciences, University of Tulsa, Tulsa, Oklahoma

ABSTRACT

Barremian through uppermost Aptian strata from ODP Hole 641C, located upslope of a tilted fault block on the Galicia margin (northwest Spain), are syn-rift sediments deposited in the bathyal realm and are characterized by rapid sedimentation from turbidity currents and debris flows. Calcarenite and calcirudite turbidites contain shallow-water carbonate, terrigenous, and pelagic debris, in complete or partial Bouma sequences. These deposits contain abraded micritized bioclasts of reefal debris, including rudist fragments. The youngest turbidite containing shallow-water carbonate debris at Site 641 defines the boundary between syn-rift and post-rift sediments; this is also the boundary between Aptian and Albian sediments.

Some Aptian turbidites are partially silicified, with pore-filling chalcedony and megaquartz. Adjacent layers of length-fast and -slow chalcedony are succeeded by megaquartz as the final pore-filling stage within carbonate reef debris. Temperatures of formation, calculated from the oxygen isotopic composition of the authigenic quartz, are relatively low for formation of quartz but are relatively warm for shallow burial depths. This quartz cement may be interpreted as a rift-associated precipitate from seawater-derived epithermal fluids that migrated along a fault associated with the tilted block and were injected into the porous turbidite beds. These warm fluids may have cooled rapidly and precipitated silica at the boundaries of the turbidite beds as a result of contact with cooler pore waters. The color pattern in the quartz cement, observed by cathodoluminescence and fluorescence techniques, and changes in the trace element geochemistry mimic the textural change of the different quartz layers and indicates growth synchronism of the different quartz phases.

Fluorescence petrography of neomorphosed low-Mg-calcite bioclasts in the silicified turbidites shows extensive zonation and details of replacive crystal growth in the bioclasts that are not observed by cathodoluminescence. Fluorescence microscopy also reveals a competitive growth history during neomorphism of the adjacent crystals in an altered carbonate bioclast.

Barremian-Aptian background pelagic sediments from Hole 641C have characteristics similar to pelagic sediments from the Blake-Bahama Formation described by Jansa et al. (1979) from the western North Atlantic. Sediments at this site differ from the Blake-Bahama Formation type locality in that the Barremian-Aptian pelagic sediments have a higher percentage of dark calcareous claystone and some turbidites are silicified at Site 641. The stable isotopic composition of the pelagic marlstones from Site 641 is similar to those of other Berriasian-Aptian pelagic sediments from the Atlantic.

INTRODUCTION

Site 641, drilled on Ocean Drilling Program (ODP) Leg 103, is upslope of a tilted fault block that is within a series of fault blocks associated with a passive margin. These blocks appear as a sequence of steps ascending from the eastern North Atlantic Basin up the outer portion of the Galicia margin on the northern Iberian continental margin (Fig. 1A). The fault block immediately downslope from that of Site 641 was drilled at Sites 639 and 638 (Fig. 1B), with a recovery of pre-rift and lower syn-rift sediments, respectively. Site 641 was drilled with the objective of completing the stratigraphic history of syn- and post-rift sedimentation.

Strata recovered at Site 641 record the evolution of the Galicia margin in a region that responded as the basin/margin interface between sedimentation from the continent, allochthonous sedimentation from thriving Cretaceous reefs upslope from the site, and pelagic sedimentation from the oceanic realm. This chapter describes the redeposition and diagenesis, including silicification, of shallow-water carbonates in the Barremian through Aptian strata recovered from Hole 641C.

Site 641 is at a water depth of 4636 m, and coring recovered strata from six lithologic units associated with the upper section of syn-rift sediments and the lower section of post-rift sediments. Three holes were drilled at this site, but sediment was recovered only at Holes 641A and 641C (Fig. 2). Hole 641A penetrated Pleistocene slumped brown clay, marl, and calcareous ooze from a depth of 0 to 15.7 m below seafloor (mbsf) that overlies Upper Cretaceous brown clay to 53.6 mbsf (Unit I), black zeolitic clay from 53.6 to 53.9 mbsf (Unit II), and Cenomanian and upper Albian calcareous clay and marl from 53.9 to 64 mbsf (Subunit IIIA). Hole 641C recovered Albian black and green laminated claystone from 151 to 202.6 mbsf (Subunit IIIB); upper Aptian greenish gray marlstone interbedded with conglomerates of granule-sized shallow-water limestone clasts from 202.6 to 218.3 mbsf (Unit IV); Aptian thin calcarenite turbidites, silicified limestone conglomerate, black claystone, and greenish gray marlstone containing slump and debris-flow deposits of pelagic claystone pebbles and shallow-water limestone clasts from 218.4 to 250.6 mbsf (Unit V); and lower Aptian marlstone to middle/upper Barremian thin silt turbidites, limestone sand turbidites, and debris-flow deposits containing shallow-water debris and pelagic claystone pebbles from 250.6 to 305.2 mbsf (Unit VI). The sections from each drill hole are separated by an unsampled interval (see Fig. 2).

Redeposited sediments in the form of turbidites and debris-flow deposits are common throughout Aptian-Barremian strata in Hole 641C (Units IV through VI). These turbidites and debris-flow deposits are the subject of this chapter, with emphasis on diagenesis of the shallow-water carbonate debris.

[1] Boillot, G., Winterer, E. L., et al., 1988. *Proc. ODP, Sci. Results*, 103: College Station, TX (Ocean Drilling Program).

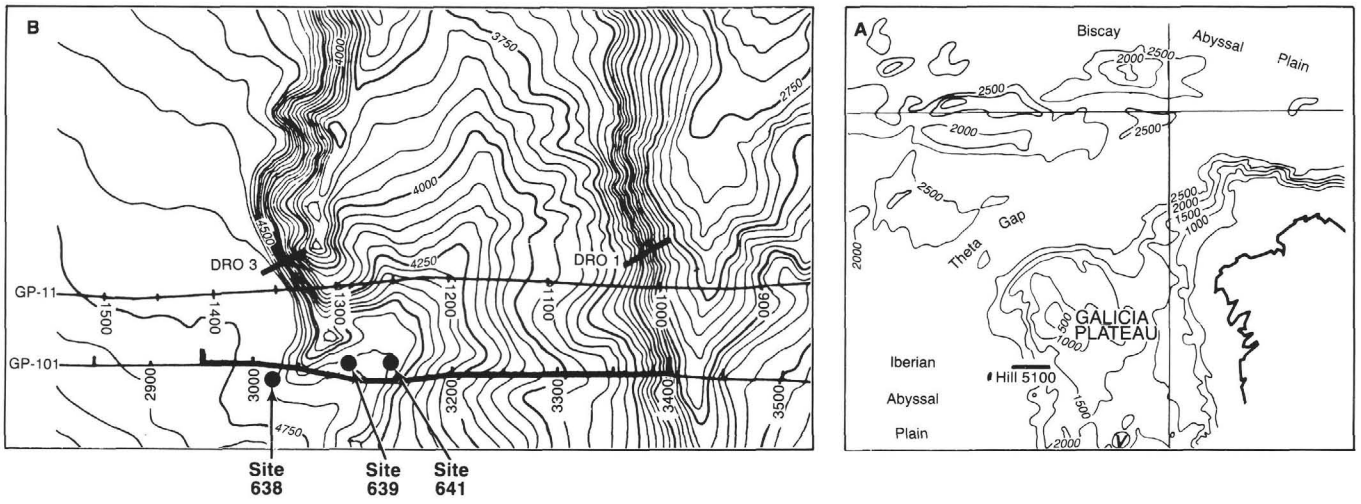

Figure 1. **A.** Location map of the Galicia margin on the northern Iberian continental margin along the eastern North Atlantic Basin. Thick line indicates area of enlargement shown in Figure 1B. **B.** Site 641 is immediately upslope from the fault block on which Sites 638 and 639 are drilled.

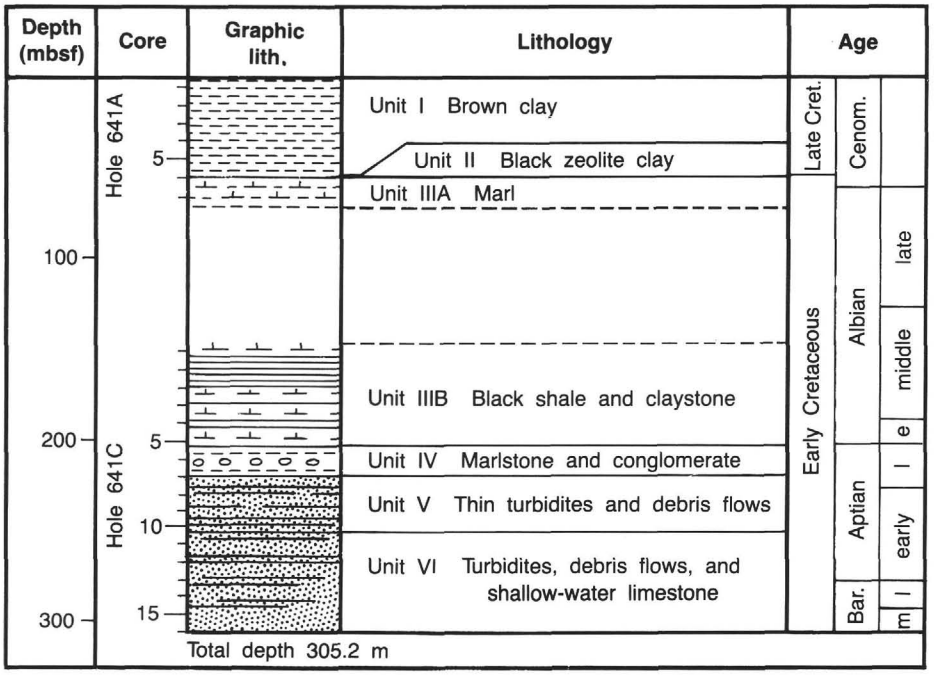

Figure 2. Stratigraphic summary of Site 641 (Holes 641A and 641C).

Methods

The distribution of turbidites and debris-flow conglomerates was surveyed, and representative samples of background pelagic sediment, redeposited shallow-water limestones, and gravity-flow deposits containing diagenetic features of silicification were selected. ODP policy does not permit more than one-quarter of the volume of the core recovered to be sampled. Because several researchers may be interested in a particular core interval, sample selection can be limited. The resulting small volume (5–10 cm^3) of sample curtails the complexity of the analytical scheme beyond routine petrographic analyses.

Mineralogy of cements and bioclasts was determined by X-ray diffraction (XRD) using a Norelco diffractometer with a high-energy, Ni-filtered, Cu-K_α source. Observations with a Coates and Welter scanning electron microscope (SEM) revealed details of the morphology of cement and preservation of radiolarians in the pelagic background sediment.

Cement stratigraphy was investigated by cathodoluminescence and blue-violet fluorescence microscopy. Cathodoluminescence, the emission of light during electron bombardment (Smith and Stenstrom, 1966), and fluorescence, the emission of a longer wavelength of light than the wavelength of the excitation light (van Gijzel, 1979), are forms of luminescence that may occur in minerals with a suitable electron configuration. Variations in the trace element chemistry as a result of crystal zonation, an abundance of fluid or solid inclusions, or differences in mineralogy can produce different colors of luminescence. Fluorescence microscopy also proved helpful in revealing relic microstructure of altered bioclasts, which aided identification of fauna and flora.

Electron microprobe analysis was used to determine variations in the chemical composition of an altered carbonate bioclast and quartz cement. For analysis of carbonate grains, thin sections were coated with silver following the method of Smith (1986) to inhibit thermal decomposition of the carbonates during electron bombardment and to maintain excellent spatial resolution. Coating carbonates with silver, rather than

carbon, increases analytical precision and lowers the detection limits for trace elements in carbonate rocks (Smith, 1986). An ARL five-spectrometer electron microprobe was operated at an accelerating potential of 20 kV and a sample current of 10 nA for calcite analysis, using a 1-μm focused beam. Counting times on the peak and the high and low background sides of the peak were 10 s for Ca and Mg, 200 s for S and Na, and 210 s for Fe, Mn, and Sr. Total counting time per point was 10.5 min, with an additional time of approximately 2 min for data reduction and driving the spectrometers and stage to the next point. Analytical time for the transect of 70 points in the calcite bioclast was approximately 14 hr. The detection limits for the trace elements in the calcite are as follows: 60 ppm Fe, 60 ppm Mn, 35 ppm S, 200 ppm Sr, and 120 ppm Na.

To analyze the quartz cement, the silver coating on the thin sections was removed, and they were recoated with carbon. The electron microprobe was operated at an accelerating potential of 20 kV and a sample current of 150 nA for quartz analysis, using a 1-μm focused beam. All trace elements in the quartz were analyzed with 200-s counting times on the peak and the high and low background sides of the peak. Analytical time for the transect of 150 points in the quartz cement was about 24 hr. The detection limits for the elements in the quartz are as follows: 20 ppm Fe, 30 ppm Al, 20 ppm K, 30 ppm Na, and 20 ppm Ti.

As a consequence of the intial small sample volume, a limited number of samples were chosen for stable isotopic analysis. Samples of turbidites containing terrigenous clastics and carbonate debris were analyzed for carbon and oxygen isotopic composition of the carbonate components. Turbidites containing no terrigenous clastics and only carbonate clasts cemented with quartz were analyzed for carbon and oxygen isotopic composition of the carbonate bioclasts as well as the oxygen isotopic composition of the quartz cement. Samples of adjacent pelagic marlstone were also chosen for bulk-rock isotopic analysis.

Carbon dioxide evolved from 10–15 mg of carbonate sediment reacted with 100% phosphoric acid was extracted for isotopic analysis following the procedure outlined by McCrea (1950). The carbon dioxide gas sample was analyzed with a Micromass stable isotope ratio mass spectrometer, and carbon and oxygen isotope analyses are reported relative to the Peedee belemnite (PDB) standard, as well as the standard mean ocean water (SMOW) standard for oxygen isotopic compositions. Analytical error was no greater than ±0.2‰ for carbonate samples. Turbidite samples containing both carbonate bioclasts and quartz cement were analyzed either (1) by first extracting carbon dioxide from the carbonate component in the rock and then preparing the remaining quartz cement for analysis or (2) by drilling specific bioclasts for carbon and oxygen isotope analysis and acid etching the rock to remove the remaining carbonate bioclasts, after which the quartz cement was prepared for oxygen isotope analysis. Quartz cement samples were analyzed following the method of Clayton and Mayeda (1963) on the mass spectrometer used for the carbonate analyses. Oxygen isotope compositions of the quartz samples are reported relative to the SMOW standard.

Flat chips of silicified rudstone were polished on each side to enhance visibility of fluid inclusions in the quartz cement and used for microthermometry. Standard techniques discussed in Roedder (1984) and Shepard et al. (1985) were used to determine homogenization temperatures of hydrocarbon inclusions on a Linkham heating and freezing stage.

RESULTS

Distribution and Description of Turbidites and Debris-Flow Deposits

Redeposited sediments in the form of turbidites and debris-flow deposits are common throughout Hole 641C Aptian to Barremian strata from Cores 103-641C-6R through 103-641C-16R (Units IV through VI). The turbidites are recognized using several diagnostic criteria: (1) occurrence of shallow-water debris in a pelagic environment, (2) discordant ages of microfossils, (3) partial or complete Bouma sequences, and (4) moderately to poorly sorted beds that contain a significant amount of clay-sized material. Hole 641A did not recover any turbidites containing shallow-water debris. Gravity-flow deposits observed in the sediments from Hole 641C are considered to be representative of the actual bathyal rock sequence containing redeposited sediments. Recovery in Cores 103-641C-6R through 103-641C-16R averaged 71.8%, which is good for rotary drilling.

Microturbidites, generally averaging less than 1 cm in thickness, are present throughout Units V and VI (see "Site 641" chapter; Shipboard Scientific Party, 1987b). The microturbidites are fine-grained sandstones and siltstones that grade upward into calcareous claystone and are commonly capped by light gray marlstone (Fig. 3). The beds are laminated and represent T_{d-e} of the Bouma sequence.

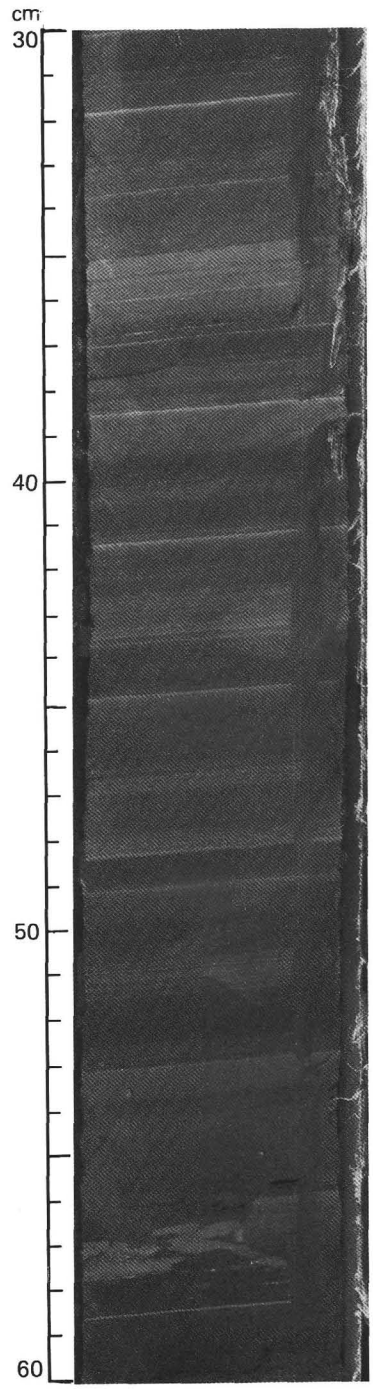

Figure 3. Microturbidites commonly found in lithologic Units V and VI are composed of fine-grained sandstones and siltstones that grade upward into calcareous claystone and are capped by light gray marlstone. Sample 103-641C-16R-3, 30–60 cm.

Thicker turbidites (≥2 cm) and other gravity-flow deposits occur in intervals in Units IV (Sample 103-641C-6R-3, 58 cm, to Section 103-641C-7R, CC), V (Samples 103-641C-8R-1, 0 cm, to 103-641C-11R-3, 26 cm), and VI (Sample 103-641C-11R-3, 26 cm, to Section 103-641C-16R, CC) in Hole 641C. These macroturbidites contain shallow-water carbonate, terrigenous, and pelagic debris. Debris-flow deposits adjacent to turbidites contain pelagic lithoclasts and shallow-water bioclasts whereas isolated debris-flow deposits contain only pelagic lithoclasts of clayey limestone and marlstone. Slumped intervals of claystone are common throughout Hole 641C. The turbidites vary from 2 to 45 cm in thickness and are classified as carbonate sandstones or calcarenites (Table 1 and Fig. 4). The thicknesses of immediately adjacent turbidite layers, that is, those lacking interbedded pelagic sediment, are added together and displayed in Figure 4 as one horizon at depth below seafloor. The relative frequency of turbidites decreases with increasing depth. Although thinner turbidites are present throughout the units, the relative abundance of thicker calcarenite layers increases with depth (Fig. 4).

Unit IV, the uppermost syn-rift unit, contains frequent calcirudite to calcarenite deposits, predominantly of shallow-water origin (Table 1). The following types of bioclasts are identified: rudists and other bivalves, echinoderms, orbitolinids, mollusks, algae, bryozoans, and corals. The turbidite boundaries are in contact with either greenish marlstone or gray-green calcareous claystone. Average thickness of turbidites in Unit IV is only 9.3 cm. The upper boundary of Unit IV is placed at the top of the uppermost occurrence of calcirudite; this is also the Aptian to Albian transition based upon foraminifer and nannofossil biostratigraphy.

Sediments of Unit V contain microturbidites and macroturbidites; some of the macroturbidites in the upper part of this unit are silicified. The silicification of calcareous turbidites has been reported previously only from ODP Leg 101, Site 634 (McClain and Freeman-Lynde, 1987), whereas chert and silicified pelagic limestone are commonly reported in Deep Sea Drilling Project (DSDP) studies. In Sections 103-641C-8R, CC, through 103-641C-9R-1, a total 35 cm of silicified shallow-water conglomerates was recovered. This silicified rudstone-packstone contains abraded rudistid, molluscan, and echinoderm fragments cemented by quartz in the form of chalcedony and megaquartz (Figs. 5 and 6). This silicified interval represents multiple pulses of turbidites composed primarily of T_{a-c} in the Bouma sequence; no *in-situ* pelagic strata were recovered between silicified turbidite layers. These layers are overlain by a debris-flow deposit of partially silicified skeletal packstone that includes a 17-cm-thick block of marlstone containing microturbidites (Fig. 7). The debris-flow sequence is succeeded by 230 cm of slumped, bioturbated, black and greenish black organic-rich claystone (Fig. 8). The 35 cm of silicified conglomerate is underlain by laminated black claystone containing pyritized radiolarians.

The macroturbidites of Unit V typically have an incomplete Bouma sequence and contain shallow-water carbonate debris (Table 1). Pyritized radiolarians are common throughout this unit (Fig. 9) and are commonly found at the base of fine-grained sandstones and siltstone laminae in the microturbidites. Overlying the Unit V silicified interval are rare, shallow-water carbonate turbidites (see Fig. 4 and Table 1), whereas the microturbidites occur with increasing frequency.

Unit VI, the lowermost unit in Hole 641C, contains several macroturbidites and microturbidites intercalated with a grayish marlstone interval. Terrigenous sediments in the macroturbidites consist of quartz and feldspar, as well as lithic fragments of quartzite, low-grade metamorphosed sandstone, biotitic granite, and schist. The thickest macroturbidites, greater than 40 cm in thickness, are found in this unit (see Fig. 4). The lowermost occurrence of a turbidite with a complete T_{a-e} Bouma sequence and containing shallow-water debris is from 42 to 84 cm in Section 103-641C-13R-5 (Table 1). This macroturbidite begins with a scoured base associated with a pebbly mudstone (T_a) and a coarse-grained calcarenite containing clay chips and coal debris, which grade upward into medium- to fine-grained calcarenite displaying climbing ripples and overlain by gray bioturbated marlstone (T_e). The lowermost macroturbidite (Fig. 10) occurs in middle/upper Barremian strata and consists of a thin bed containing neomorphosed carbonate debris and terrigenous debris (including detrital quartz, plant fragments, and biotite) in a micrite matrix (see Table 1). Debris-flow deposits (Fig. 11) and slump deposits (Fig. 12), both of intrabasinal origin, become more common in this unit. The debris-flow deposits contain redeposited ovoid pebbles and cobbles of marlstone, limestone, and claystone that are similar to the background pelagic sediment.

Macroturbidites from Unit VI have a greater abundance of detrital quartz, feldspar, and lithic fragments than the overlying units. The macroturbidites are generally thickest and have the best developed Bouma sequences in lower Aptian strata from Unit VI. Unit V, on the other hand, is dominated in the lower part by microturbidites with few macroturbidites. Thicker and better developed macroturbidites appear in the upper part of Unit V, and the microturbidites diminish in frequency and eventually disappear. The macroturbidites in the upper part of Unit V are primarily silicified calcirudites and calcarenites. In Unit IV, calcarenite pulses increase in frequency and contain less terrigenous sediment (with the exception of the 56–64 cm interval in Section 103-641C-6R-3; see Table 1) than those turbidites found in Units V and VI. Furthermore, these younger calcarenites are thinner and have fewer sedimentary structures. The contact between Unit IV and Subunit IIIB is defined by the uppermost macroturbidite and the lowermost deposit of Albian pelagic strata, respectively.

Description of Background Pelagic Sediments

The Barremian to Aptian strata are composed of interbedded pelagic sediment (claystone, marlstone, and clayey limestone) with rudstone to calcisiltite turbidites and debris-flow deposits. Of the general trends observed in the background pelagic sediments that surround the macroturbidites in Hole 641C, the most dramatic is an increase of calcium carbonate and a decrease of carbonaceous claystone with increasing depth. Subunit IIIB consists predominantly of greenish gray and black laminated claystone that varies in carbonate content from 0% to 11%, generally constituting less than 4% of the dried sediment weight (see carbonate-bomb data in "Inorganic Geochemistry" section of the "Site 641" chapter; Shipboard Scientific Party, 1987b). No turbidites or any trace of shallow-water carbonate debris is present in this unit. Unit IV is more calcareous and greener in color than those sediments recovered in Subunit IIIB. Greenish gray marlstone becomes more prevalent and remains common throughout Unit IV. In Unit V, the sediments continue to have a high percentage of calcium carbonate. The occurrence of carbonaceous claystone decreases significantly in this unit. At the Unit V/Unit VI boundary, marlstone and clayey limestone comprise more than 50% of the recovered sediment, whereas above that boundary they are less than 50%. This gray marlstone and clayey limestone range in carbonate content from 42% to 83% of the dried sediment weight and dominate the pelagic sediment thoughout Unit VI. These gray pelagic sediments distinctly lack macrofossils and are either laminated or moderately to extensively bioturbated.

Radiolarians are rare in the lower Aptian and Barremian pelagic sediment (Unit VI); an increase in the abundance of radiolarians occurs in the uppermost lower Aptian strata of Unit V

Table 1. Distribution of macroturbidites from Hole 641C.

Sample	Depth (mbsf)	Lithology	Description
Unit IV			
6R-3, 56–64 cm	202.56–202.64	Calcirudite	Skeletal packstone containing shallow-water carbonate debris consisting of orbitolinids, echinoderms, algae, and bivalves. Quartz and lithic fragments are rare. Bouma sequence: T_a
6R-3, 115–127 cm	203.15–203.27	Calcirudite	Skeletal packstone similar to the overlying sample but with trace amounts of quartz, lithic fragments, and angular pelagic lithoclasts of green marlstone and black claystone.
6R-3, 136–150 cm	203.36–203.50	Calcarenite	Packstone containing bioclasts of echinoderms, mollusks, bryozoans, and larger foraminifers. Bouma sequence: T_a
7R-1, 126–150 cm, to 7R-2, 0–5 cm	209.96–210.25	Calcirudite to calcarenite	Grainstone to packstone containing coarse-grained, micritized shallow-water debris: orbitolinids, echinoderms, algae, rudists, and other bivalves. Also contains a trace amount of quartz grains and radiolarians. Bouma sequence: T_a
7R-2, 15–21 cm	210.35–210.41	Calcarenite	Same as the overlying sample but contains medium- to fine-grained bioclasts. Bouma sequence: T_b
7R-2, 36–39 cm	210.56–210.59	Calcarenite	Graded shallow-water debris.
7R-2, 46–57 cm	210.66–210.77	Calcarenite to calcisiltite	Coarse carbonate sand grading into finely laminated calcisiltite. . Bouma sequence: T_{c-d}
Unit V			
8R-1, 50–60 cm	218.90–219.00	Calcarenite	Calcareous sandstone grading upward into calcisiltite and marlstone. Bed has sharp base and gradational top. Bouma sequence: T_{b-e}
8R-1, 76–83 cm	219.16–219.23	Calcarenite	Similar to overlying turbidite.
8R, CC (7–24 cm) to 9R-1, 0–5 cm	227.83–228.05	Silicified rudstone	Contains rudists, *Inoceramus*, and echinoderms that have been partially or completely silicified. Pore-filling quartz in the form of chalcedony and megaquartz is present. Bouma sequence: T_a
9R-1, 6–20 cm	228.06–228.20	Silicified grainstone	Silicified carbonate sand containing micritized rudists, echinoderms, and orbitolinids, as well as abundant peloids. Terrigenous grains, such as detrital quartz, are present in trace amounts. Quartz is also present as authigenic pore-filling cement and partially replacing rudists. Bouma sequence: T_{b-c}
9R-2, 6–14 cm	229.56–229.64	Calcarenite	Fine-grained carbonate sand containing peloids, quartz, feldspar, and biotite grains. Quartz is also present as pore-filling cement.
9R-3, 70–74 cm	231.70–231.74	Calcarenite	Laminated carbonate sandstone.
9R-3, 84–90 cm	231.84–231.90	Calcarenite	Packstone containing peloids, radiolarians, and lithic fragments. Bouma sequence: T_{b-e}
10R-3, 140–143 cm	242.00–242.03	Calcarenite	Peloids, benthic foraminifers, ostracodes, biotite, plant debris, and quartz grains in a sparry matrix. Terrigenous debris and clay are concentrated in several thin layers (<1 mm).

Table 1 (continued).

Sample	Depth (mbsf)	Lithology	Description
Unit V (cont)			
10R-6, 20–26 cm	245.30–245.36	Calcarenite	Carbonate sand bed.
11R-2, 73–78 cm	249.53–249.58	Quartzose calcarenite	Fine- to medium-grained carbonate sand bed with less than 15% quartz grains. Bouma sequence: T_{b-c}
11R-2, 100–102 cm	249.80–249.82	Quartzose calcarenite	Fine-grained carbonate sand bed; similar to the overlying turbidite. Bouma sequence: T_{c-e}
11R-2, 114–118 cm	249.94–249.98	Quartzose calcarenite	Medium-grained carbonate sand bed grading upward to a fine-grained carbonate. Bouma sequence: T_{c-e}
Unit VI			
11R-3, 120–150 cm, to 11R-4, 0–17 cm	251.50–251.97	Calcirudite to calcarenite	Quartz-bearing packstone to wackestone that contains bioclasts of corals, rudists, orbitolinids, bivalves, echinoderms, and algae. Clay, biotite, feldspars, and metamorphic rock fragments are also present in the packstone to wackestone. The lowermost section of this turbidite is composed of a calcirudite containing pelagic lithoclasts of clayey limestone and marlstone, plant debris, and quartz grains. Bouma sequence: T_{a-d}
12R-3, 0–2 cm	259.90–259.92	Calcarenite	Intraclasts, recrystallized bioclasts, and benthic foraminifers in wackestone. The terrigenous components in this packstone are quartz grains, biotite, and plant debris.
12R-3, 115–132 cm	261.05–261.22	Calcarenite	Packstone containing peloids, recrystallized bioclasts, intraclasts, abundant benthonic foraminifers, *Inoceramus*, and algae in a sparry matrix. Terrigenous components consist of quartz, biotite, and plant debris. Bouma sequence: T_{a-b}
12R-4, 133–137 cm	262.73–262.77	Calcarenite	Medium-grained grading up to fine-grained mixed carbonate and terrigenous clastic sandstone.
12R-6, 142–150 cm, to 12R-7, 0–5 cm	264.40–264.53	Calcarenite	Siliclastic-bearing packstone containing bivalves, algae, orbitolinids, rudists, *Inoceramus*, corals, and a trace amount of glauconite. Terrigenous components consist of biotite, quartz grains, and quartzite. Bouma sequence: T_{a-c}
13R-3, 12–19 cm	269.62–269.68	Calcarenite	Packstone consisting of peloids, benthic foraminifers, mollusks, echinoderms, and glauconite in a sparry matrix. Terrigenous components consist of quartz, feldspar, and biotite grains. Bouma sequence: T_{c-d}
13R-3, 20–26 cm	269.70–270.76	Calcarenite	Similar to the overlying turbidite. Bouma sequence: T_{b-c}
13R-3, 27–55 cm	269.77–270.05	Calcarenite	Coarse-grained grading upward to a medium-grained packstone containing peloids, benthic foraminifers, intraclasts, echinoderms, mollusks, algae, and glauconite. Terrigenous components consist of lithic fragments, quartz, feldspar, and biotite grains. Bouma sequence: T_{a-c}

Table 1 (continued).

Sample	Depth (mbsf)	Lithology	Description
Unit V (cont)			
13R-5, 42–84 cm	272.92–273.34	Pebbly mudstone and calcarenite	Scoured base associated with a pebbly mudstone and a coarse-grained calcarenite, grading upward into a medium- to fine-grained calcarenite exhibiting climbing ripples; this sequence is overlain by bioturbated marlstone. The calcarenite is a packstone similar in content to the overlying turbidite but with the addition of clay chips and coal debris in the coarse-grained calcarenite. Bouma sequence: T_{a-e}
14R-1, 14–24 cm	276.34–276.44	Siliclastic calcarenite	Packstone with abundant quartz and feldspar grains and bioclasts in a micritic matrix. Bioclasts consist of bivalves, benthic foraminfers, rudists, and algae. Bouma sequence: T_a
14R-5, 60–67 cm	282.80–282.87	Calcarenite	Fine-grained calcarenite containing intraclasts in a sparry matrix that grades up into light gray marlstone.
16R-6, 98–100 cm	303.98–304.00	Calcarenite	Fine-grained wackestone containing recrystallized carbonate debris, quartz grains, plant debris, and biotite grains.

(see "Barrel Sheets," "Site 641" chapter; Shipboard Scientific Party, 1987b). Radiolarians are common to abundant in upper Aptian (Unit IV) through Albian strata (Subunit IIIB). Surface dissolution of the ornamentation used for detailed taxonomic identification has occurred in radiolarian specimens from Subunit IIIB through Unit VI, and some specimens are infilled with chalcedony.

Laminated claystone-marlstone and bioturbated marlstone-clayey limestone can be discriminated on the basis of their primary sedimentary structures. The two end-members are distinctly laminated or bioturbated, but in several locations, a transitional form is observed in which bioturbation has not completely destroyed the laminations. Any of these claystone-marlstone-clayey limestone fabrics may abut against a turbidite.

Bioturbation can be detected in thin section by patterns generated from either the increased concentrations of radiolarians within burrows and the patchiness of micritic matrix or by color and textural difference resulting from increased clay content in a burrow. Radiolarians, as well as burrows, are sometimes flattened and oriented parallel to bedding, indicating compaction.

A microstructure of elongate pods appears in the laminated pelagic sediment. The origin of these elongate pods may be the diagenetic precipitation of silica and/or compositional differences in constituent grains during deposition of the sediment. In thin section, these structures are resolved to be isolated pods aligned parallel to the bedding plane, appearing in hand specimen as distinctly laminated sediment. The outlines of some pods are enhanced by compaction of surrounding clay and organic debris. The laminated limestones contain a terrigenous silt component of fine-grained mica and quartz and also of land plant debris.

Several grayish green clay layers, less than 1 mm thick, occur in Aptian strata from Unit VI. These layers contain altered glass shards and may represent ash layers (see "Sediment Lithology" section, "Site 641" chapter; Shipboard Scientific Party, 1987b). All of the background pelagic deposits in Units IV through VI contain variable amounts of detrital clays; usually the darker the color, the greater percentage of clay. The percent organic carbon content in a laminated pelagic sediment is always higher than the organic carbon content of adjacent bioturbated pelagic sediment (see "Organic Geochemistry" section, "Site 641" chapter; Shipboard Scientific Party, 1987b).

Geochemistry

Table 2 lists the carbon and oxygen isotopic composition of shallow-water carbonate debris extracted from turbidites, a pelagic lithoclast in a debris-flow deposit, and the background pelagic bioturbated marlstone, as well as the oxygen isotopic composition of pore-filling quartz cement in silicified rudstone and grainstone turbidites. Descriptions of the turbidites from which the samples were taken for isotopic analysis are listed in Table 1. Figures 13 and 14 show the oxygen and carbon isotopic composition of the bioclasts and the marlstone plotted against depth below seafloor. From this small data base, there appears to be a slight trend toward a lighter oxygen and carbon isotopic composition of the bioturbated marlstone with increasing depth. The isotopic composition of the bioclasts also mimics the same trend, with the exception of bioclasts from two of the three silicified turbidites sampled. These bioclasts are significantly lighter in their oxygen isotopic composition (Fig. 13). The carbon isotopic composition of two samples from the same silicified turbidite also indicate a distinct shift to a negative value (see Table 2 and Fig. 14).

The oxygen isotopic composition of three pore-filling quartz cement samples are +17.1‰, +25.1‰, and +28.5‰ (SMOW); the +17.1‰ and +25.1‰ values are the lightest oxygen isotope signatures of the whole isotope data set (see Table 2). The very light oxygen isotopic composition of Sample 103-641C-9R-1, 0–4 cm, can not be explained as contamination with detrital quartz because detrital quartz was not observed in thin sections or in the hand specimen during sampling of this specific turbidite. In Sample 103-641C-9R-1, 16–20 cm, detrital quartz is observed in thin section. This sample was inspected for an area that did not contain detrital quartz and, therefore, would be ap-

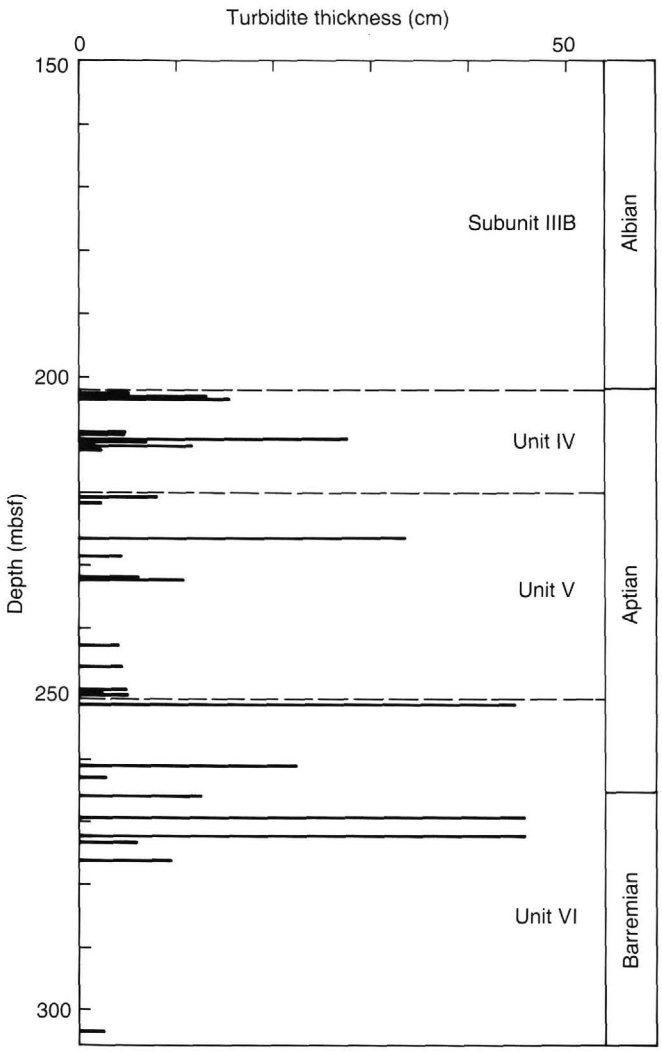

Figure 4. Macroturbidite thickness plotted against depth.

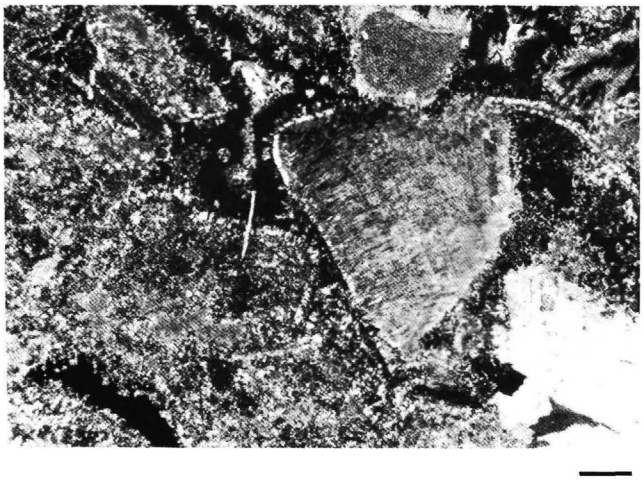

Figure 5. Silicified rudstone containing micritized bioclasts and abraded molluscan and echinoderm fragments cemented by quartz. Some bioclasts are partially replaced by quartz. Crossed nicols. Bar scale represents 0.5 mm. Sample 103-641C-8R, CC (9–11 cm).

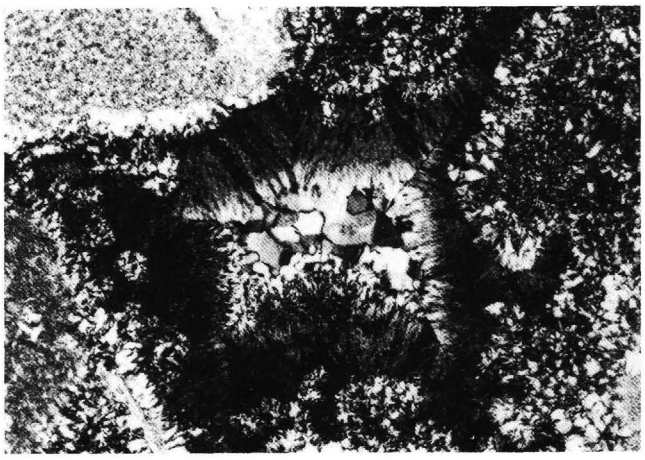

Figure 6. Pore-filling quartz cement in the form of chalcedony and megaquartz. Crossed nicols. Bar scale represents 0.1 mm. Sample 103-641C-8R, CC (13–15 cm).

propriate for subsampling for isotopic analysis of the authigenic quartz. Detrital quartz contamination of the isotope Sample 103-641C-9R-1, 16–20 cm, is doubtful because the quartz cement was carefully sampled during analysis of the specimen under a stereomicroscope.

Assuming that the pore-filling quartz cement was precipitated in isotopic equilibrium with the surrounding pore waters, these three oxygen isotope values may be entered into paleotemperature equations derived for quartz by Clayton et al. (1972) and Knauth and Epstein (1976). Possible temperatures of formation of the authigenic quartz cement are calculated using values of 0.0‰ and −1.0‰ for the waters of formation (Table 3). The assumption is made that the quartz is in isotopic equilibrium with seawater or with a hydrothermal fluid derived from seawater. This assumption appears to be justified because of the initial high porosity and permeability of calcarenite and rudstone turbidites, which should favor high water/rock ratios. In addition, the contemporaneous interstitial waters of nearby sediments from the same lithologic units in this drill hole are chemically very similar to seawater (see Haggerty and Fisher, this volume). The pore waters from which the quartz cement precipitated may have been similar to seawater; therefore, these water values are chosen because 0.0‰ corresponds to modern seawater, and a depletion of 1 per mil is used for Cretaceous seawater on the assumption that the polar ice volume was negligible during the Cretaceous (Shackleton and Kennett, 1975).

The calculated temperatures of formation for the authigenic quartz are relatively low, ranging from 36° to 135°C (see Table 3). These temperatures, calculated from the oxygen isotopic composition of the quartz, may be compared to microthermometry data from fluid inclusions. Only two fluid inclusions of an appropriate size for visual observation were found in the last stage of pore-filling quartz cement in Sample 103-641C-8R, CC (13–15 cm). These two primary fluid inclusions contained a shrinkage bubble and hydrocarbons in the megaquartz and yielded homogenization temperatures of 64.0° and 69.9°C. The temperature of formation of the quartz, calculated from the oxygen isotopic composition, is in good agreement with these homogenization temperatures. A slightly warmer temperature, greater than 100°C, is calculated from the oxygen isotopic composition of Sample 103-641C-9R-1, 0–4 cm, which is from a turbidite lacking detrital quartz that is in the middle of the interval of silicified turbidites.

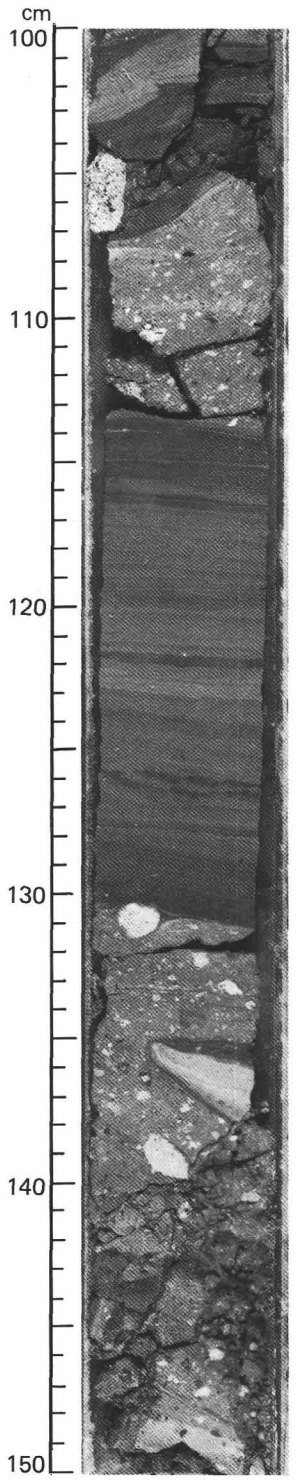

Figure 7. A skeletal packstone debris-flow deposit, which also includes a block of marlstone composed of microturbidites displaying evidence of microfaulting, overlying a silicified turbidite. Sample 103-641C-8R-4, 100–150 cm.

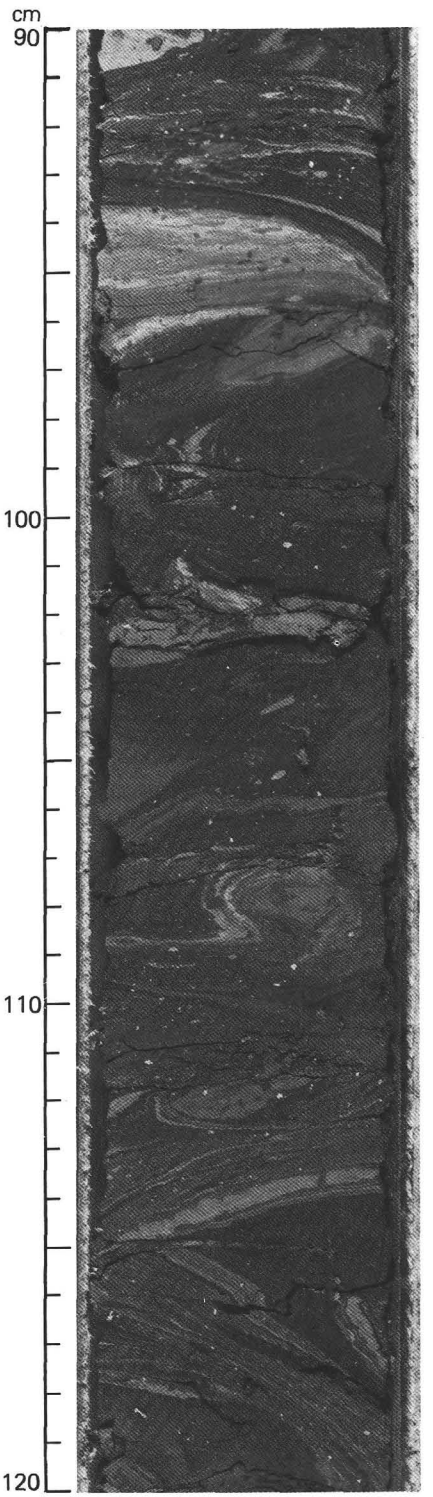

Figure 8. Slump deposit composed of black and greenish black organic-rich claystone that overlies the strata shown in Figure 7. Sample 103-641C-8R-3, 90–120 cm.

In the silicified rudstone the quartz cement is well developed and completely occludes the pores. The bioclasts are coated and invaded with small spherulitic splays of chalcedony (zone I; Fig. 15) that were subsequently covered with one or two layers of chalcedony (zones II and III; Fig. 15). The first layer of chalcedony (zone II) is composed of thin fibers and is optically length fast (i.e., the *c*-axis is perpendicular to the fibers), and the second pore-filling layer of chalcedony (zone III) is composed of slightly thicker fibers, approaching bladed, and is optically length slow. Sutured boundaries are observed within individual isopachous layers of chalcedony as the fibers converge from the corners of the pores (Fig. 15). Pores not completely

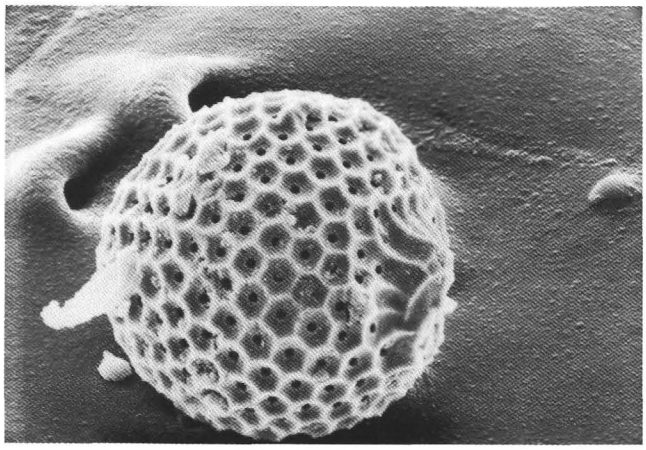

Figure 9. SEM photo of a pyritized radiolarian, which are commonly found in the base of the microturbidites. Bar scale represents 20 μm. Sample 103-641C-9R-1, 35–36 cm.

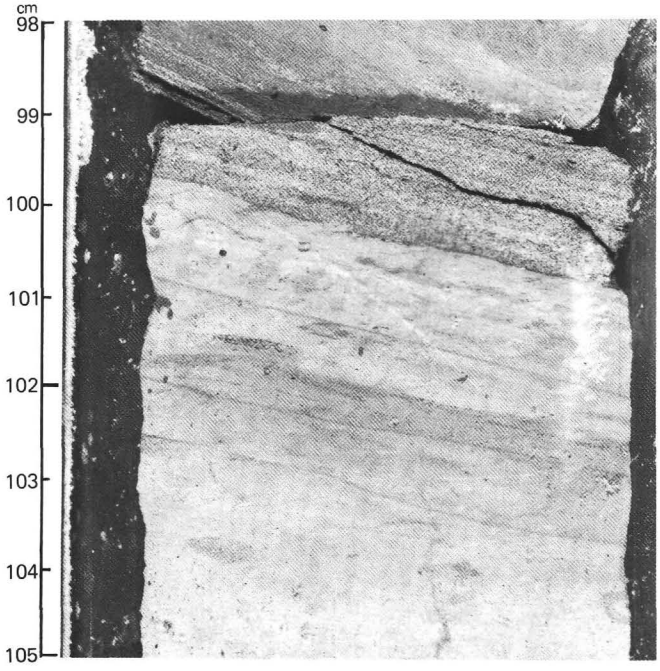

Figure 10. Lowermost macroturbidite and underlying bioturbated marlstone in Barremian age strata of lithologic Unit VI. Sample 103-641C-16R-6, 98–105 cm.

filled with chalcedony (zone III) have an additional precipitate of megaquartz appearing as the final pore-filling stage (zone IV; Fig. 15).

Cathodoluminescence and fluorescence analysis of the pore-filling quartz displayed slightly different colors for each zone of quartz illustrated in Figure 15B. The variation in the luminescence color of the different quartz layers indicates growth synchronism of each layer, and potentially, a change in the trace element chemistry of the pore waters during precipitation of the quartz.

Electron microprobe analysis was conducted to determine the trace element chemistry of each layer of quartz. Figure 16 displays the variability of Al, Fe, K, Na, and Ti across 150

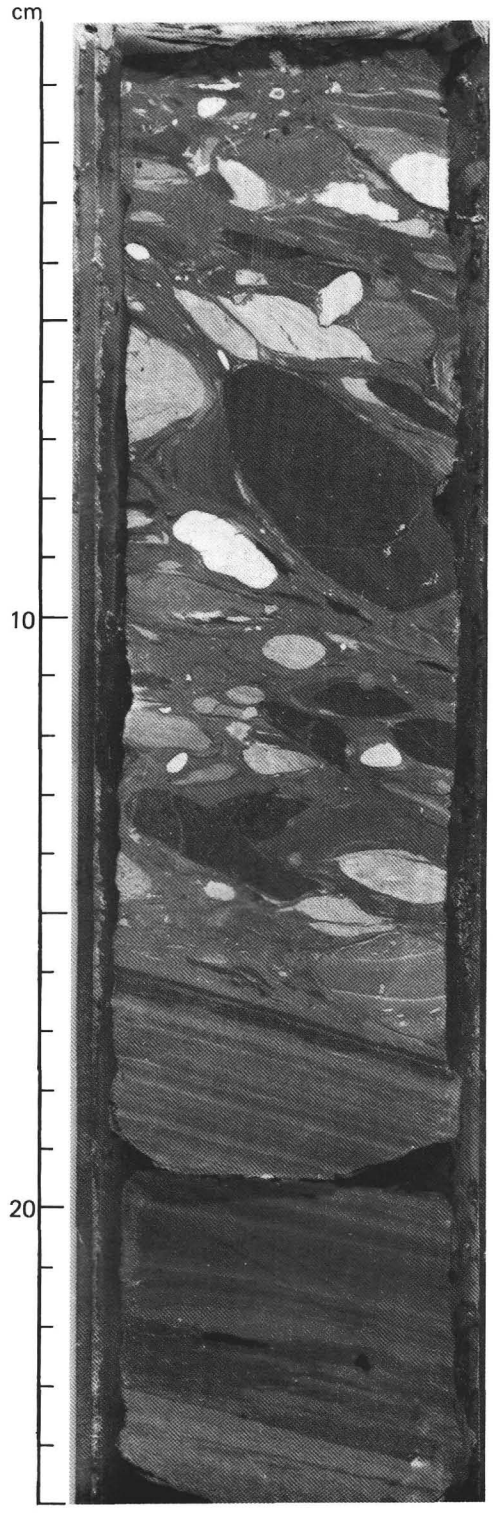

Figure 11. Debris-flow deposit containing pelagic lithoclasts in lithologic Unit VI. Sample 103-641C-15R-3, 0–25 cm.

points in the pore-filling quartz, with the zones labeled. Al and Ti show a variable pattern irrespective of the zone; if the concentration increases greatly in zones II or III on the left side of Figure 16, it does not increase significantly in zones II or III on the right side of the figure. This irregular pattern may be the result of high Al and Ti content in clays or other minerals that can

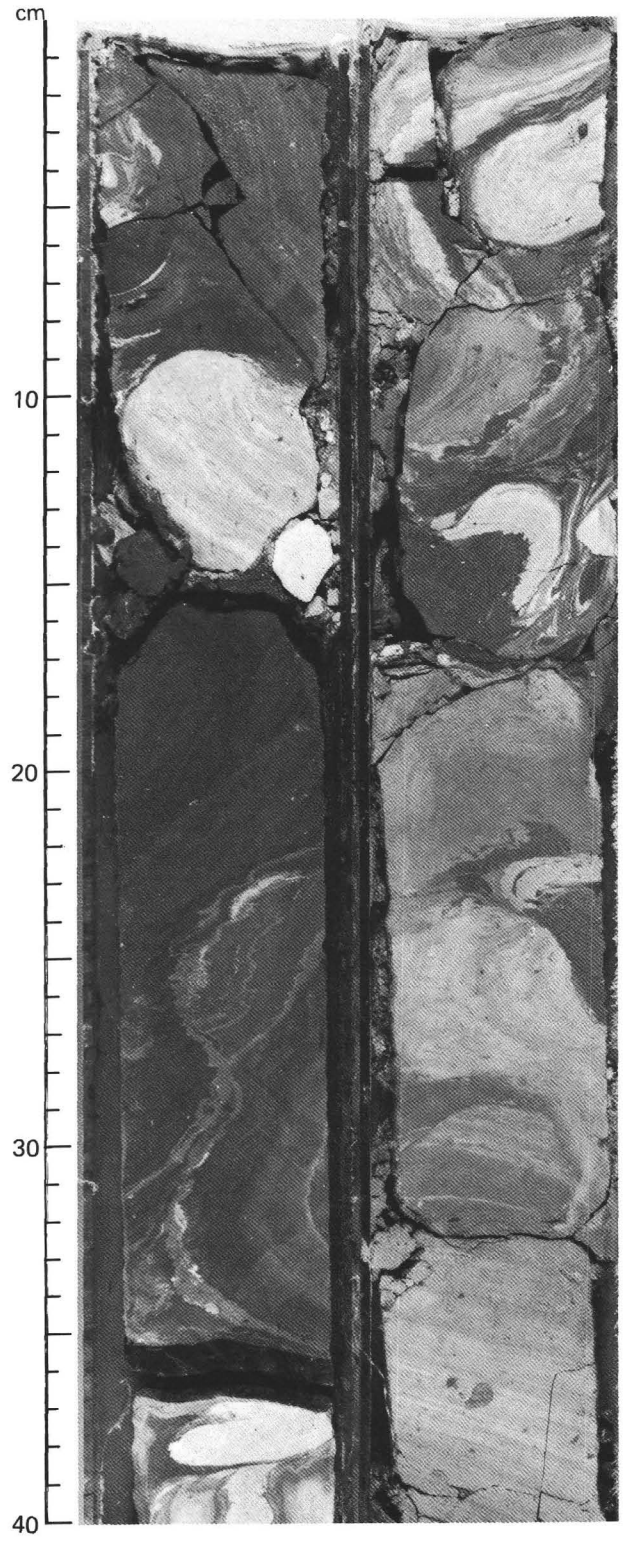

Figure 12. Extensive slump deposit of intrabasinal origin in the 0–40-cm interval in Sections 103-641C-15R-4 and 103-641C-15R-5.

occur as inclusions within or between the fibrous chalcedony. However, there does appear to be a sympathetic relationship of Ti and Na.

The trace elements that do show a consistent pattern in their variation are Fe, K, and Na. Figure 17 is a plot of the transect of 150 analyses, with all three elements on the same graph. Table 4

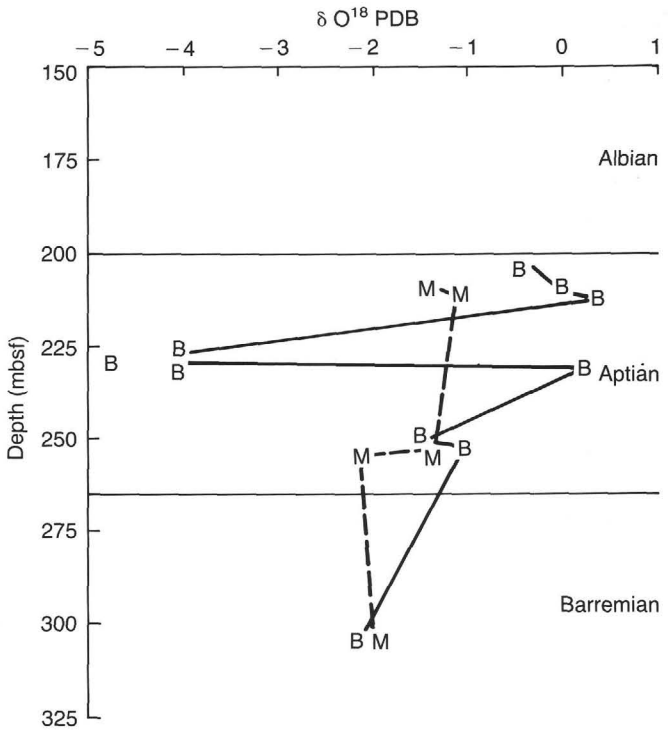

Figure 13. Plot of $\delta^{18}O$ analyses listed in Table 2 vs. depth. B = bioclasts; M = marlstone.

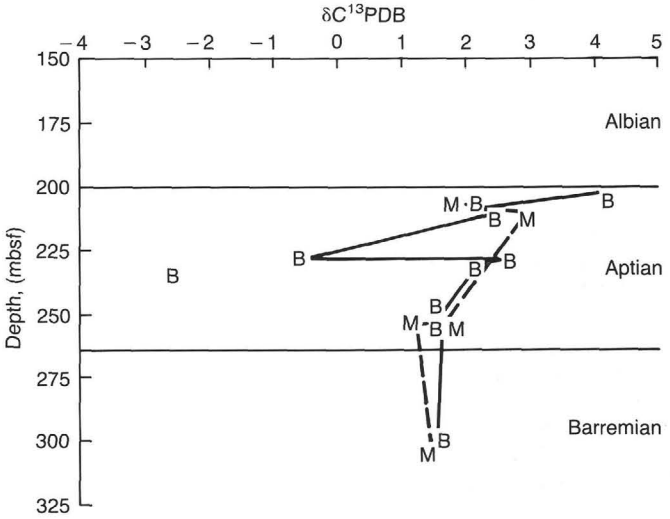

Figure 14. Plot of $\delta^{13}C$ analyses listed in Table 2 vs. depth. B = bioclasts; M = marlstone.

lists the average concentration of these three elements in each zone. The difference in luminescence between the two layers of chalcedony, thin and thicker fibers, is emphasized by the difference in the concentrations of these elements between zones II and III.

Irrespective of the zone, Fe, K, and Na increase or decrease in synchrony for each analysis (Fig. 17). Megaquartz (zone IV) displays the greatest variablity in concentration and has the highest average concentration of all three elements (see Table 4). The chalcedony layers, zones II and III, have the next highest concentration of these elements, but zone III has a lower concentration than zone II. The fibrous splays of quartz (zone I) have the

Table 2. Stable isotope analyses of samples from Hole 641C.

Sample	Description	$\delta^{13}C^a$	$\delta^{18}O^a$	$\delta^{18}O^b$
6R-3, 62–64 cm	Shallow-water debris in turbidite	+4.1	−0.4	+30.0
7R-1, 110–113 cm	Bioturbated marlstone	+1.9	−1.4	+29.0
7R-1, 135–137 cm	Shallow-water debris in turbidite	+2.1	+0.0	+30.4
7R-2, 0–2 cm	Shallow-water debris in turbidite	+2.4	+0.3	+30.7
7R-2, 4–7 cm	Bioturbated marlstone	+2.9	−1.2	+29.2
8R, CC (13–15 cm)	Shallow-water debris in turbidite	−0.5	−4.0	+26.3
	Shallow-water debris in turbidite	−3.1	−4.9	+25.4
	Pore-filling quartz cement			+28.5
9R-1, 0–4 cm	Shallow-water debris in turbidite	+2.6	−4.1	+26.2
	Pore-filling quartz cement			+17.1
9R-1, 16–20 cm	Shallow-water debris in turbidite	+2.2	+0.2	+30.6
	Pore-filling quartz cement			+25.1
11R-3, 132–134 cm	Shallow-water debris in turbidite	+1.6	−1.5	+28.9
11R-3, 148–150 cm	Shallow-water debris in turbidite	+1.6	−1.1	+29.3
11R-4, 0–5 cm	Pelagic lithoclast in debris flow	+1.5	−1.4	+29.0
11R-4, 115–117 cm	Bioturbated marlstone	+1.1	−2.2	+28.1
16R-6, 98–100 cm	Shallow-water debris in turbidite	+1.5	−2.1	+28.2
16R-6, 100–102 cm	Bioturbated marlstone	+1.4	−2.0	+28.3

[a] PDB standard.
[b] SMOW standard.

Table 3. Temperature of formation of quartz cement in Hole 641C.

Sample	$\delta^{18}O$	Waters of formation values			
		0.0‰[a] (°C)	−1.0‰[a] (°C)	0.0‰[b] (°C)	−1.0‰[b] (°C)
8R, CC (13–15 cm)	+28.5	55	49	41	36
9R-1, 0–4 cm	+17.1	135	125	118	108
9R-1, 16–20 cm	+25.1	73	67	59	53

[a] Equation from Clayton et al. (1972).
[b] Equation from Knauth and Epstein (1976).

lowest concentration of these elements (Table 4). The morphology of the quartz may govern the concentrations of these elements in the crystal or the concentrations of inclusions within or between the crystals. The morphology of the chalcedony easily lends itself to trapping inclusions between the fibers, whereas the megaquartz has a cloudy or dirty appearance from the high abundance of microinclusions within the crystal.

Cathodoluminescence and fluorescence petrography conducted on the silicified rudstone also revealed the diagenetic history of some altered bioclasts. Small areas in the central portions of these neomorphosed bioclasts luminesced red during bombardment with an electron beam, but cathodoluminescence did not indicate a detailed chemical variation in the stratigraphy of the replacement spar. Fluorescence petrography, however, shows extensive zonation and details of neomorphic crystal growth in the bioclast.

Many of the neomorphosed bioclasts contain mosaics of low-Mg-calcite spar (Fig. 18). Cathodoluminescence does not reveal any details of the growth or transformation of these features, whereas fluorescence petrography shows what appears to be large crystals with numerous fluorescent bands (Fig. 19). A careful comparison of Figures 18 and 19, taken of the exact same

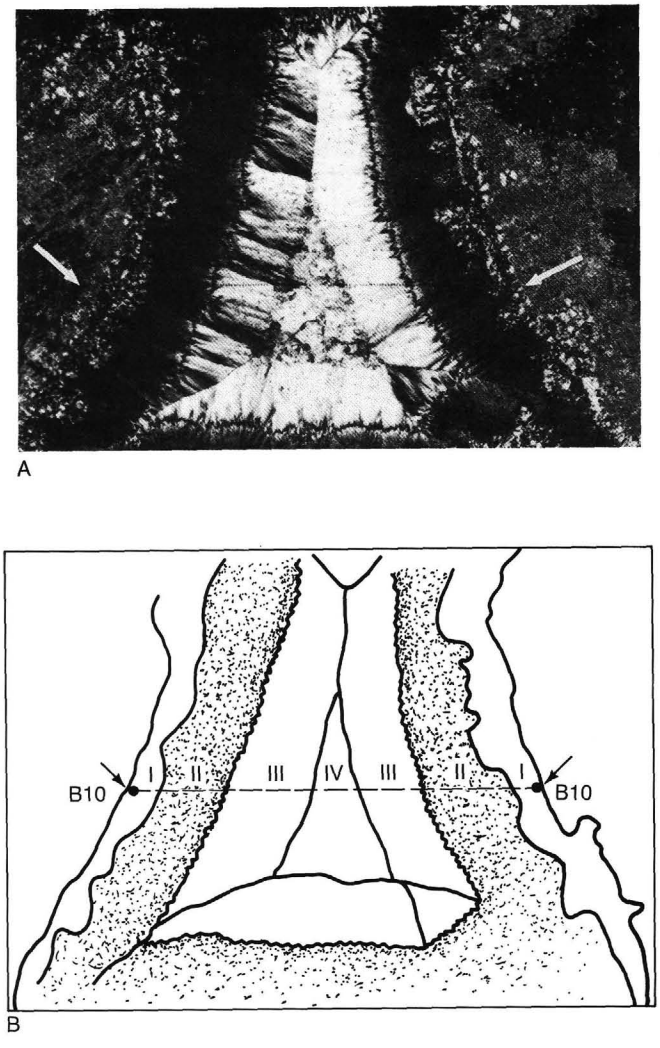

Figure 15. **A.** Photomicrograph of silicified rudstone showing stages of pore-filling quartz. Outer dark layer of chalcedony is length fast and corresponds to zone II in Figure 15B. Inner light layer of chalcedony is length slow and corresponds to zone III in Figure 15B. Arrows point to beginning and end of the electron microprobe transect. Crossed nicols. Bar scale represents 0.25 mm. Sample 103-641C-8R, CC (13–15 cm). **B.** Sketch of Figure 15A indicating the edges of micritized bioclasts (BIO) and the different zones of pore-filling quartz cement. Zone I: spherulitic splays of fibrous quartz coating and invading the micritized bioclasts. Zone II: layer of chalcedony that appears dark in Figure 15A. Zone III: layer of chalcedony that appears light in Figure 15A. Zone IV: megaquartz as final pore-filling cement. Transect of electron microprobe analyses indicated by dashed line.

area of the thin section, reveals numerous fluorescent bands that are continuous across grain boundaries. A competitive growth history has occurred at the same rate in adjacent crystals during neomorphism, thereby giving the impression in fluorescence petrography of unusually large, and slightly deformed, crystals.

Complex alteration of a bioclast is revealed using fluorescence microscopy in Sample 103-641C-8R, CC (9–11 cm) (Fig. 20). The earlier stages of neomorphism are near the micritized rim of the bioclast and generally show an alternation of green and dark green banding. There is an abrupt change in the central region of the altered bioclast. A series of luminescent bands ranging from yellow to green to black are adjacent to several mi-

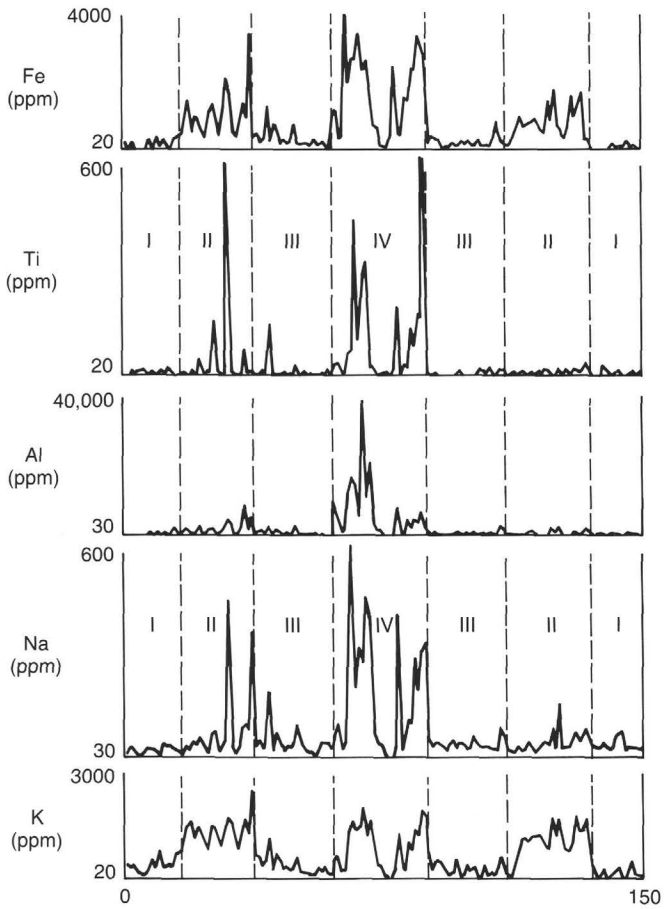

Figure 16. Trace element concentrations in the 150-point quartz-cement transect shown in Figure 15. Roman numerals correspond to the zonation labels in Figure 15B.

cropores, and from the distribution and shape of this area in Figure 20, this is interpreted as the last area of calcite precipitation.

The difference in fluorescence colors may indicate a change in the trace element geochemistry of the crystals as they grew. Electron microprobe analysis was conducted on this neomorphosed bioclast along a transect of 70 points. An enlarged area of the transect, in Figure 21, shows details of thin zones of crystalline growth. Careful, detailed observation was required to decipher the color band associated with each analysis; elemental averages associated with the colors are presented in Table 5. In the neomorphosed bioclast, high concentrations of Fe and Mn are found in the terminal black band, whereas the other colors have much lower concentrations of Fe, and Mn is below the detection limit. Moderate concentrations of Na and S are present throughout the neomorphosed bioclast (Table 5). A lower Mg content is detected in the yellow and black bands than in the green and dark green bands. The fluorescent color bands appear to reflect changes in the trace element composition of the mineral.

DISCUSSION

Environments of Deposition of Barremian-Aptian Sediments on the Galicia Margin

General trends are observed in the Barremian-Aptian pelagic strata, which are composed of bioturbated or laminated gray marlstone and encompass the turbidites. The most dramatic trend is a decrease of calcium carbonate and an increase of carbonaceous claystone from the Barremian (Unit VI) to the Aptian strata (Unit IV). Evidence from foraminifers (see "Biostratigraphy" section, "Site 641" chapter; Shipboard Scientific Party, 1987b) indicates a change from a Barremian environment above the carbonate compensation depth (CCD) to a late Aptian environment above or near the CCD in the bathyal realm. The Albian strata of Subunit IIIB do not have abundant calcareous foraminifers. This may be a consequence of a shallowing CCD, or subsidence of the site below the CCD, environmental conditions related to deposition of black claystones, or a combination of these factors.

The ash layers in Aptian strata from Unit VI may have contributed silica to the surrounding waters in the past. The apparent change in abundance of the radiolarians from Barremian through Albian strata may be related to an increase in surface-water productivity (from upwelling and/or increased availability of silica from volcanism associated with rifting), to dissolution of carbonate components in the sediments, or to both.

Microturbidites, in Units VI and V, are interpreted to represent redeposition of fine-grained hemipelagic sediment, includ-

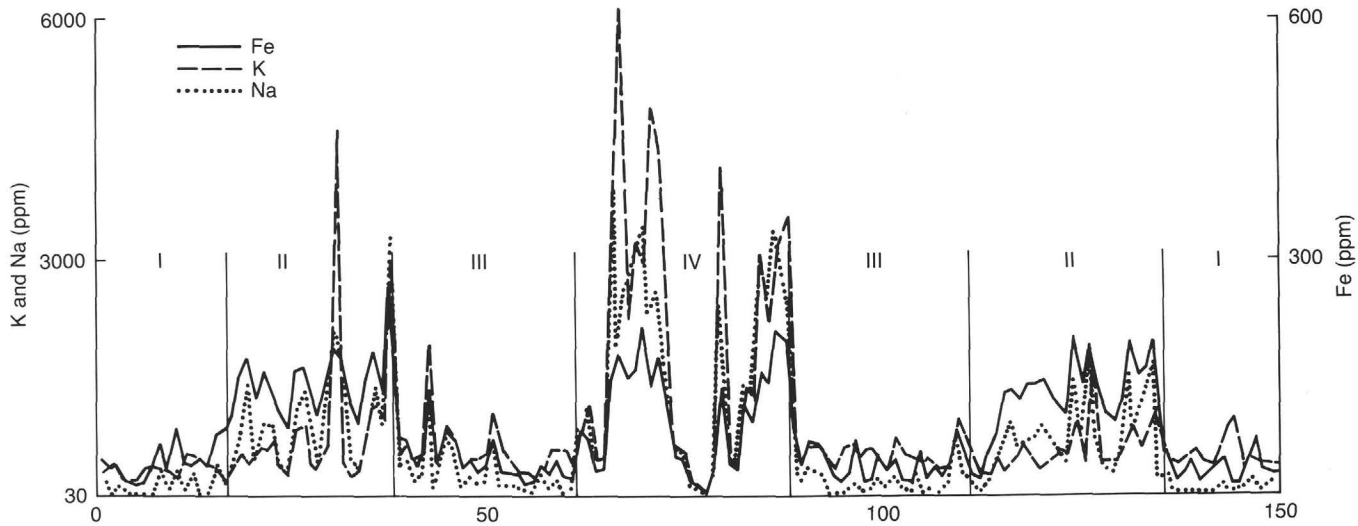

Figure 17. Transect of 150 microprobe analyses across the pore-filling quartz shown in Figure 15A. Roman numerals correspond to zonation labels in Figure 15B.

Table 4. Average elemental concentrations in quartz cement from Sample 103-641C-8R, CC (13–15 cm). Zones are designated in Figures 15–17.

Zone	Fe (ppm)	K (ppm)	Na (ppm)
I: fibrous splays	40	340	100
II: chalcedony	70	1300	830
III: chalcedony	50	400	220
IV: megaquartz	190	970	1500

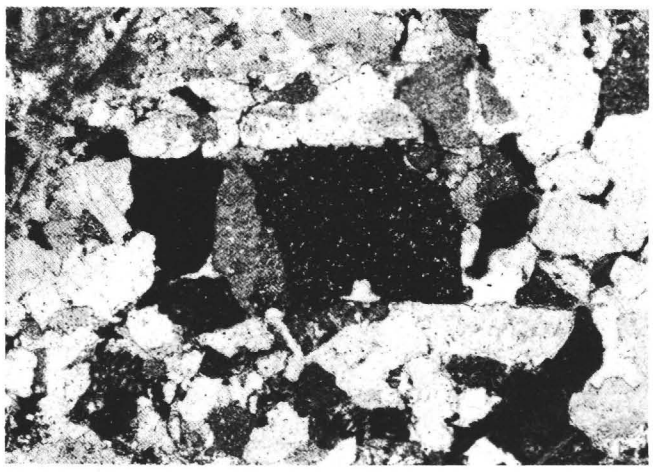

Figure 18. Mosaic of calcite spar within a neomorphosed bioclast. Chalcedony has also infilled some small pores between spar. Crossed nicols. Bar scale represents 0.1 mm. Sample 103-641C-8R, CC (9–11 cm).

Figure 19. Fluorescence petrography enhances the competitive growth history of the crystals in the same area as shown Figure 18. Blue-violet fluorescence. Bar scale represents 0.1 mm. Sample 103-641C-8R, CC (9–11 cm).

ing pyritized radiolarians, in a bathyal environment during the middle Barremian through early Aptian. The microturbidites are the lowermost turbidites recovered from Hole 641C, with the oldest recovered macroturbidite at Site 641 consisting of shallow-water, terrigenous, and plant debris (Unit VI; Sample 103-641C-16R-6, 98–100 cm). Deposition of thin macroturbidites occurred throughout the Barremian to Aptian, while the deposition of thicker calcarenite layers was more prevalent during the early Aptian in this bathyal environment. In addition to the shallow-water carbonate debris found in all the macroturbidites, those deposited during the Barremian through early Aptian (Unit VI) have a greater abundance of detrital quartz, feldspar, and lithic fragments than the younger turbidites. Some of the

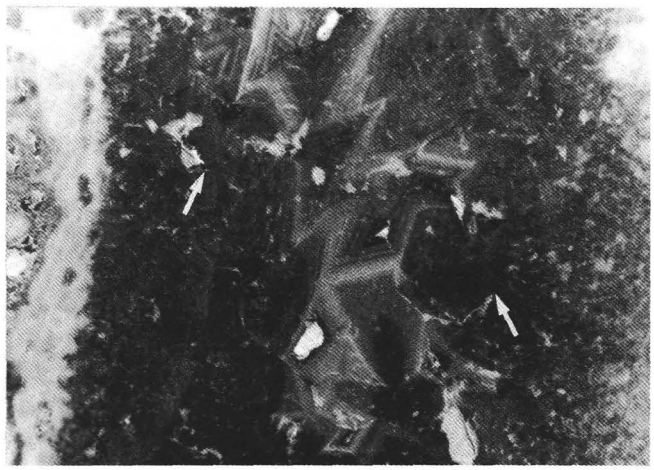

Figure 20. Complex alteration of a bioclast displaying crystallization stratigraphy. Arrows indicate beginning and end points of the electron microprobe transect. Blue-violet fluorescence. Bar scale represents 0.1 mm. Sample 103-641C-8R, CC (9–11 cm).

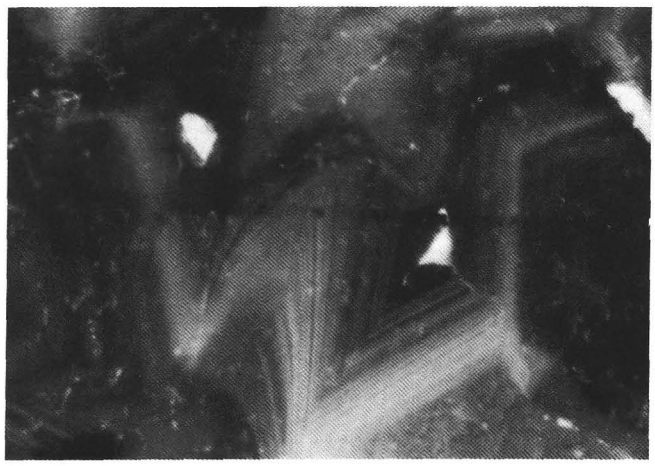

Figure 21. Close-up of an area in Figure 20 showing details of thin zones of crystalline growth with several points from the microprobe transect. Bright white areas are micropores in the sample. Blue-violet fluorescence. Bar scale represents 0.05 mm. Sample 103-641C-8R, CC (9–11 cm).

Table 5. Neomorphosed calcite bioclast from Sample 103-641C-8R, CC (13–15 cm).

Zone	Mg (ppm)	Fe (ppm)	Mn (ppm)	Na (ppm)	Sr (ppm)	S (ppm)
Yellow	2400	70	B.D.	300	B.D.	120
Green	3100	130	B.D.	450	B.D.	200
Dark green	3100	180	B.D.	330	220	260
Black	2000	4400	5300	500	B.D.	320

Note: Zones correspond color of fluorescence observed using a blue-violet light source. B.D. = below detection limit.

macroturbidites deposited during the latest early Aptian have been subsequently silicified. During the late Aptian, shallow-water-derived calcirudites and calcarenites continued to be deposited; however, they abruptly disappeared at the end of the Aptian.

The frequency of macroturbidites increases from Barremian (Unit VI) through Aptian strata (Unit IV). Slumped intervals of claystone are common throughout Hole 641C, but isolated debris-flow deposits and slumps that lack shallow-water debris are more common in Barremian strata (Unit VI) and are interpreted as having been derived from sediments on the slope within the basin. Turbidites and debris-flow deposits containing carbonate debris, which are interpreted as having been derived from sediments on the shelf, occur in Barremian-Aptian strata.

The redeposited sediments recovered at Site 641 expand our knowledge of the environments associated with the development of this passive margin. Valanginian through Barremian sediments recovered at Site 638 (see Fig. 1) are lower syn-rift sediments, characterized by abundant terrigenous sand turbidites and calcareous claystone turbidites and interbedded in pelagic marlstone and calcareous claystone. The Barremian through the uppermost Aptian sediments in Hole 641C are the upper syn-rift sediments (Cores 103-641C-6R to 103-641C-16R), similarly characterized by rapid sedimentation from gravity-flow deposits, which are predominantly turbidites. The youngest occurrence of a turbidite containing shallow-water carbonate debris at Site 641 defines the boundary between syn-rift and post-rift sediments; this is also the boundary between Aptian and Albian sediments.

The gravity-induced deposits reflect changes in the tectonic history of the Galicia margin. The terrigenous turbidites deposited during the Valanginian-Hauterivian at Site 638 contain sand grains that indicate derivation of material from a granitic or granodioritic terrain, with a minor amount of schist and low-grade metamorphosed sandstone (see "Sediment Lithology" section, "Site 638" chapter; Shipboard Scientific Party, 1987a). The material could have been transported to the site by way of canyons associated with a river outlet or by a conduit associated with materials accumulated on the shelf. Calcareous claystone turbidites were deposited during the Barremian at Site 638 and are continued at Site 641 as Barremian debris-flow deposits containing pelagic lithoclasts and slumps that lack shallow-water debris. Aptian debris-flow deposits containing some shallow-water debris were deposited adjacent to macroturbidites at Site 641. During the Valanginian-Barremian, the margin may have been compartmentalized from increased tilting of the fault blocks. The increased tilting might account for the unstable nature of sediments on the slope, which was frequently disrupted by slumping and gravity-flow currents. These syn-rift sediments rapidly began to infill the half-grabens.

Macroturbidites from the syn-rift Unit VI at Site 641 have a greater abundance of detrital quartz, feldspar, and lithic fragments of quartzite, low-grade metamorphosed sandstone, biotitic granite, and schist than the overlying syn-rift units. The lowermost occurrence of a turbidite with a complete Bouma sequence at Site 641 is in Unit VI, and it contains terrigenous clastics, coal debris, and shallow-water debris. The greater abundance of terrigenous sediments in macroturbidites of Unit VI for all of Hole 641C may suggest deposition closer to a land source, greater relief and erosion of a tectonically uplifted land area during the late Barremian to early Aptian, or a combination of these factors. The ash layers in the Aptian pelagic strata support the notion of tectonism at the time of deposition.

From the Barremian through early Aptian, Site 641 was associated with a eustatic sea-level rise (Vail et al., 1977). The duration of the sea-level rise corresponds to the time interval of deposition of thick macroturbidites containing terrigenous as well as shallow-water debris (Cores 103-641C-13R through 103-641C-15R) and abundant microturbidites. The terrigenous influx waned in the Aptian, possibly because this sediment became trapped by a "ponding effect" on the inner shelf. The late Aptian was characterized by a sudden drop in eustatic sea level (Vail et al., 1977), which corresponds to frequent pulses of shallow-water-derived macroturbidites. The syn-rift sediments continued to infill the half-grabens until the late Aptian. The uppermost turbidite in Unit IV is a calcarenite that also contains terrigenous debris from 56 to 64 cm in Section 103-641C-6R-3 (see Table 1), which indicates that during the latest Aptian some terrigenous material was reaching the edge of the shelf. The Albian experienced a subsequent sea-level rise (Vail et al., 1977).

The presence of rudist fragments and clasts of other framework organisms (see Table 1) in these macroturbidites indicates the existence of a carbonate buildup on the Galicia margin during the Barremian-Aptian. Lower Cretaceous carbonate buildups have also been documented in other locations in the Atlantic, Gulf of Mexico, Caribbean, and Mediterranean regions (Paulus, 1972; Coates, 1973; Perkins, 1974; Schlager, 1980).

Several factors might have caused the termination of turbidite deposition during the subsequent rapid rise in sea level in the Albian. The terrigenous sediment supply may have decreased because erosion lowered the relief of the land or as the result of thermal cooling and subsidence of the land area in this post-rift stage. Any available terrigenous sediments were probably trapped on the inner shelf during this subsequent transgression. The outer shelf had a carbonate buildup during the Early Cretaceous, as indicated by the abundance of carbonate debris in the Barremian-Aptian calcarenites. Although the carbonate buildup was still a possible source for debris, the drop in sea level in the Aptian may have resulted in an exposure of the carbonate buildup or an alteration of the reef environment to less than optimum growth conditions. Exposure of a reef allows meteoric lithification to occur, which would curtail the production of fine or coarse carbonate talus associated with prograding reefs during high sea-level stands (Schlager and Ginsburg, 1981). Schlager (1980) suggested that the drowning of a shallow-water carbonate buildup would require a slight drop followed by a rapid rise of sea level. Hallock and Schlager (1986) have suggested a mechanism that would inhibit the rapid accretion rates of carbonate reefs and therefore permit them to drown immediately after a sudden sea-level drop followed by a rapid rise of sea level. They suggested that excess nutrient availability from terrestrial runoff can suppress reef growth before the arrival of terrigenous clastics or that even excess nutrients from changes in upwelling patterns may be sufficient to inhibit reef growth. The uppermost turbidite in upper Aptian strata is a calcarenite containing terrigenous debris, which indicates that some terrigenous material was reaching the edge of the shelf during the latest Aptian. The mechanism suggested by Hallock and Schlager (1986) may explain the demise of the reef in the Aptian, and the subsequent rapid sea-level rise from the late Aptian through the Albian may have resulted in trapping the terrigenous sediment on the shelf.

The background pelagic sediments in Unit VI from Hole 641C have characteristics similar to the pelagic sediments associated with the Blake-Bahama Formation in the western North Atlantic, for which Jansa et al. (1979) described the incorporation of turbidites with pelagic sediments to be not unusual. At DSDP Site 391, the type locality for the Blake-Bahama Formation, clastic intervals are found that contain siliciclastics, plant debris, and ooids (Jansa et al., 1979). Robertson and Bliefnick (1983) also report the occurrence of redeposited clastics in the Blake-Bahama Formation in the Blake-Bahama Basin at DSDP Site 534. The occurrence of mixed terrigenous and shallow-water carbonate turbidites within the formation at Site 641 indi-

cates the presence of an active reef on the tilted block from the Galicia margin in the eastern Atlantic during the Barremian-Aptian. The sediments at this site differ from the Blake-Bahama Formation type locality in that the Barremian-Aptian pelagic sediments have a higher percentage of dark calcareous claystone and some of the turbidites are silicified at Site 641.

Diagenesis of Barremian-Aptian Sediments from the Galicia Margin

The isotopic data (Fig. 22) are compared with data from the Blake-Bahama Formation from Berriasian-Valanginian pelagic sediments of DSDP Site 603 on the New Jersey continental rise in the western North Atlantic (Baltuck, 1987; Haggerty, 1987; Prezbindowski and Pittman, 1987) and from Barremian-Aptian pelagic sediments of DSDP Site 398 along the Iberian margin in the eastern North Atlantic (Arthur et al., 1979). The stable isotopic composition of the pelagic marlstones from Site 641 plot within the fields of these Berriasian-Aptian pelagic sediments. On the basis of petrographic evidence and carbon and oxygen stable isotopic composition, the background pelagic sediments from Site 641 have undergone only burial diagenesis.

With the exception of the bioclasts from two of the three silicified turbidites, the isotopic composition of micritized bioclasts also mimics the same trend of lighter oxygen and carbon isotopic composition with increasing depth below seafloor (Figs. 12 and 13 and Table 2). These micritized bioclasts are significantly lighter in their oxygen isotopic composition (Fig. 13), which may may indicate that micritization occurred in warmer water, in meteoric water, or in water influenced by hydrothermal input. The carbon isotopic composition of two samples from the same silicified turbidite also indicate a distinct shift toward a negative signature (see Table 2 and Fig. 14), which is not typical for an isotopic signature of a marine carbonate. Limestones that have undergone subaerial exposure usually have a negative carbon and oxygen isotopic signature (Allan and Matthews, 1977). The carbon and oxygen isotopic signature of both micritized bioclasts from the same silicified rudstone turbidite (Sample 103-641C-8R, CC [13–15 cm]) may be debris from an Aptian reef that became subaerially exposed during the Aptian sea-level drop, or the isotopic signature may be related to another type of diagenesis.

The quartz cement samples have oxygen isotopic compositions of +17.1‰, +25.1‰, and +28.5‰. From Blatt's (1987) survey of published data on oxygen isotopes of quartz, the average quartz values are +9‰ for igneous rocks, +13‰ to +14‰ for metamorphic rocks, +11‰ for sandstones, +19‰ for shales, +20‰ for quartz overgrowths in sandstone, and +28‰ for cherts. Contamination of the quartz cement samples with terrigenous clastics has been dismissed as a cause of these light isotopic values in consideration of the sampling technique. Oxygen isotopic compositions of authigenic quartz formed during diagenesis as quartz in shale, quartz overgrowths in sandstones, and chert are closer to the compositional range of the quartz cement from the silicified turbidites in Unit V.

Burial diagenesis of argillaceous sediments releases silica during the transformation of smectite sheets to illite, but Hower et al. (1976) have shown that mud rocks appear to be a closed chemical system with respect to silica during diagenesis. Thus, it is unlikely that sufficient silica could migrate from the pelagic strata to the porous rudstones for silicification. The elongate micropods present in the laminated marlstone are diagenetic concentrations of silica that are consistent with Hower et al.'s (1976) observations.

A potential source of silica that should be discussed is the lower syn-rift sandstones recovered at Site 638 from Subunit IIIB (Samples 103-638B-35R-4, 55 cm, to 103-638B-45R, CC [25 cm] and 103-638C-1R-1, 0 cm, to 103-638C-14R, CC [30 cm]) in Hauterivian strata. These sandstones have attained the locomorphic stage (Dapples, 1962) in their diagenetic evolution in which both feldspar and quartz grains are replaced along their rims by ferroan sparry calcite ("Sediment Lithology" section, "Site 638" chapter; Shipboard Scientific Party, 1987a). In Hole 638C, these sandstones are in strata at a depth from 411.9 to 547.2 mbsf. This mechanism has not been proven as a significant contributor of silica for migration through sediments to other strata but is suitable for local silicification.

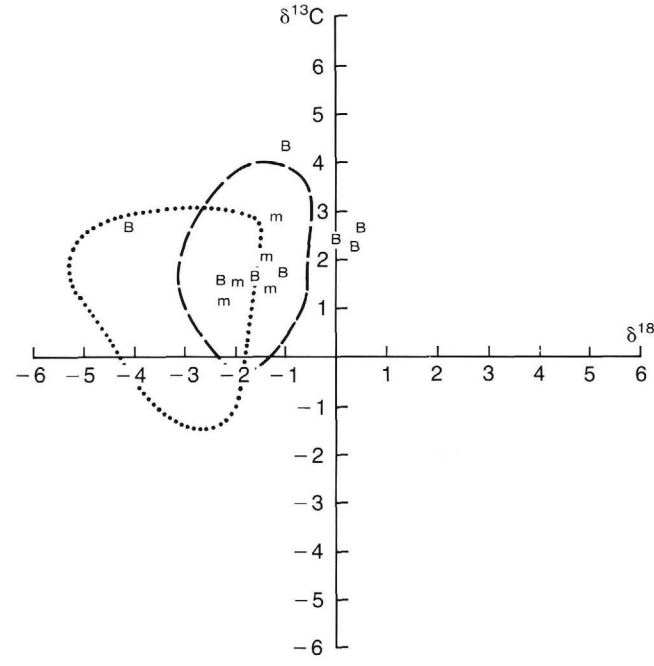

Figure 22. Crossplot of all carbon and oxygen isotope data from the carbonate samples listed in Table 2. The regions associated with the isotopic composition of Berriasian-Valanginian pelagic marlstone from DSDP Site 603 in the western North Atlantic (dashed line) and Barremian-Aptian pelagic marlstone from DSDP Site 398 in the eastern North Atlantic (dotted line) are shown for comparison. M = marlstone from Site 641; B = micritized bioclast from Site 641.

The dissolution of biogenic silica also appears to be an insufficient source for the quantity of silica present in these silicified rudstones. The radiolarians in the surrounding pelagic strata are not well preserved, as noted by surface dissolution of ornamentation used for taxonomic identification, but the radiolarians are not calcified and are commonly infilled with chalcedony. No molds of radiolarians are found in the pelagic strata. Furthermore, there is no evidence of siliceous microfossils in the silicified turbidites.

The calculated temperatures of formation for the authigenic quartz are relatively low for the formation of quartz, ranging from 36° to 135°C (see Table 3), but are relatively warm for shallow-burial depths (227.8 and 229.6 mbsf). These temperatures are also considerably higher than the temperature of normal deep-ocean water. The formation temperature of quartz calculated as greater than 100°C is from a turbidite that lacks detrital quartz (Sample 103-641C-9R-1, 0–4 cm) and is in the middle of the interval of silicified turbidites. This quartz cement may be interpreted as a rift-associated precipitate of seawater-derived epithermal fluids, which migrated along a fault associated with the tilted block and were injected into these porous turbidite beds. As the warm fluids spread to the boundaries of the beds, which are between 227.8 and 229.6 mbsf, the fluids rapidly cooled in contact with the cooler pore waters and precipitated quartz.

Inorganic formation of quartz in the marine environment is possible as a precipitate from solutions that have leached silica out of volcanic material. The inorganic formation of opal precipitates has been documented by Bertine and Keene (1975) from the Lau Basin, where hydrothermal solutions are emanating from a fracture zone offsetting the active ridge. They calculated a temperature of formation of 41°C from an oxygen isotopic composition of +31.1‰ for the opal.

The micritized bioclasts in these silicified turbidites may not have been influenced by meteoric waters in order to yield the negative isotopic values. For marine limestone experiencing contact metamorphism, increased proximity to the intrusive contact results in greater depletion in ^{13}C and ^{18}O in the isotopic composition of the limestone (Deines and Gold, 1969; Faure, 1977). If the quartz precipitated from epithermal fluids, then possibly the micritized bioclasts were affected by these fluids. This may explain the unusual isotopic signature of the three micritized bioclasts in the silicified turbidites. If an Aptian carbonate buildup was subaerially exposed, lithoclasts of limestone with textures of meteoric phreatic or meteoric vadose cements possibly were incorporated into the turbidites; however, these have not been found. In addition, one would expect to find negative carbon and oxygen isotopic signatures in other turbidite bioclasts than those that are silicified.

The pattern of luminescence color in the quartz cement, as observed by cathodoluminescence and fluorescence, mimics the textural change of the different quartz layers and indicates growth synchronism of the different quartz phases. Microprobe analysis of the trace element composition of the quartz indicates a change occurred in the chemical composition of each layer, thereby yielding different luminescent colors. The chemical contribution from inclusions can not be disregarded when analyzing the microprobe data. The obvious synchronism of Fe, K, and Na indicates either a true change in the chemical composition of the quartz or an apparent change in the chemical composition by changing the amount of inclusions. This chemical change from layer to layer may be interpreted as a change in the trace element chemistry of the pore waters during precipitation of the quartz, or it may be related to a change in the growth rate of the quartz and the subsequent entrapment of inclusions.

Fluorescence petrography also revealed a competitive growth history during neomorphism of adjacent crystals in an altered carbonate bioclast. If the color of the fluorescence band indicates a change in the composition of the calcite, then an interpretation can be made of the change in the chemistry of the waters during alteration of the bioclast.

The bioclast studied from the silicified turbidite showed a micritic rim (yellow fluorescence), with the next region within the altered bioclast displaying an alternating green and dark green banding that has a more prevalent dark green fluorescence. This region may have undergone heteroaxial transformation, the inversion of aragonite to calcite by solution and *in-situ* precipitation in an aqueous environment so that no structural correspondence between aragonite and calcite crystals is maintained. Although this region has a moderate Na and S contents, it maintains higher Sr and Mg contents than other regions of the altered bioclast. The interior region of the bioclast has several layers surrounding micropores that abruptly change from yellow to green to black. The pattern of zonation in this central region may be interpreted as a region of dissolution and subsequent reprecipitation from which the pore waters became rich in Fe and Mn. The combination of high Fe and Mn in the last-formed layer may be related to precipitation during burial within the turbidite, prior to silicification.

CONCLUSIONS

Valanginian through Barremian sediments recovered at Site 638 are lower syn-rift sediments, characterized by abundant terrigenous sand turbidites and calcareous claystone turbidites that are interbedded in pelagic marlstone and calcareous claystone. The Barremian through the uppermost Aptian sediments in Hole 641C are upper syn-rift sediments deposited in a bathyal realm and are characterized by rapid sedimentation from gravity-flow deposits. The youngest occurrence of a turbidite containing shallow-water carbonate debris at Site 641 defines the boundary between syn- and post-rift sediments; this is also the boundary between Aptian and Albian sediments.

During the Valanginian-Barremian, the margin may have been compartmentalized, with increased tilting of the fault blocks. Consequently, this tilting could have aided the development of slumping and gravity-flow currents down the slope, thereby causing syn-rift sediments to rapidly infill the half-grabens. The greater abundance of terrigenous sediments in Aptian macroturbidites suggests deposition closer to a land source, greater relief and erosion of a tectonically uplifted land area during the late Barremian to early Aptian, or a combination of these two.

The duration of the Barremian–early Aptian sea-level rise corresponds to the time interval of deposition of thick macroturbidites containing terrigenous, as well as carbonate, debris and abundant microturbidites. The terrigenous influx waned in the Aptian as the sediment became trapped on the inner shelf. The late Aptian sea-level drop corresponds to frequent pulses of shallow-water-derived macroturbidites. The presence of terrigenous debris in the uppermost Aptian turbidite indicates that some terrigenous material was reaching the edge of the shelf during the latest Aptian.

Several factors might have caused the termination of turbidite deposition in the Albian during the subsequent rapid rise of sea level. The terrigenous sediment supply may have decreased because of erosion lowering the relief of the land area or as the result of thermal cooling and subsidence of the land area in this post-rift stage. Any available terrigenous sediments were probably trapped on the inner shelf during this subsequent transgression. The carbonate buildup during the Early Cretaceous on the outer shelf was a source for debris until the drop in sea level in the Aptian resulted in either an exposure of the carbonate buildup or an alteration of the reef environment to less than optimum growth conditions.

The Barremian-Aptian background pelagic sediments from Hole 641C have similar characteristics to the pelagic sediments associated with the Blake-Bahama Formation in the western North Atlantic (Jansa et al., 1979). The stable isotopic composition of the pelagic marlstones from Site 641 is similar to those of other Berriasian-Aptian pelagic sediments from the Atlantic.

The quartz cement in the turbidites is interpreted as a precipitate from seawater-derived epithermal fluids associated with rifting, which migrated along a fault associated with the tilted block and were injected into these porous turbidite beds. These warm fluids rapidly cooled when they mingled with the cooler pore waters and consequently precipitated quartz. The pattern of luminescence color in the quartz cement, as observed by cathodoluminescence and fluorescence, and the changes in the geochemistry mimic the textural change of the different quartz layers and indicate growth synchronism of the different quartz phases.

In previous carbonate petrologic studies, the technique of cathodoluminescence has been used more prevalently than fluorescence. It has been commonly thought that cathodoluminescence was more sensitive to changes in trace element geochemistry of a mineral, whereas fluorescence has been generally used to detect hydrocarbon inclusions or to enhance microstructure of poorly preserved bioclasts (Dravis and Yurewicz, 1985). Fluorescence petrography in neomorphosed bioclasts shows extensive zonation and details of replacive crystal growth in the bioclast. This technique also reveals a competitive growth history during neomorphism of adjacent crystals in an altered carbon-

ate bioclast. The results from this study indicate that fluorescence petrography may be more helpful to carbonate petrographers than previously thought.

ACKNOWLEDGMENTS

The authors thank Michael P. Smith for aid and helpful advice with the electron microprobe analyses and Paul Franks for stimulating discussions about quartz diagenesis. This paper benefited from comments by J. S. Compton and one anonymous reviewer. Funds for this research were granted by the National Science Foundation though JOI-U.S. Science Advisory Committee.

REFERENCES

Allan, J. R., and Matthews, R. K., 1977. Carbon and oxygen isotopes as diagenetic and stratigraphic tools: surface and subsurface data, Barbados, West Indies. *Geology*, 5:16–20.

Arthur, M. A., Scholle, P. A., and Hasson, P., 1979. Stable isotopes of oxygen and carbon in carbonates from Sites 398 and 116 of the Deep Sea Drilling Project. *In* Sibuet, J.-C., Ryan, W.B.F., et al., *Init. Repts. DSDP*, 47, Pt. 2: Washington (U.S. Govt. Printing Office), 447–491.

Baltuck, M., 1987. Geochemistry, carbon and oxygen stable isotope composition, and diagenetic textural features of Lower Cretaceous pelagic cyclic sediments from the Western North Atlantic, Deep Sea Drilling Hole 603B. *In* van Hinte, J. E., Wise, S. W., Jr., et al., *Init. Repts. DSDP*, 93: Washington (U.S. Govt. Printing Office), 989–995.

Bertine, K. K., and Keene, J. B., 1975. Submarine barite-opal rocks of hydrothermal origin. *Science*, 188:150–152.

Blatt, H., 1987. Oxygen isotopes and the origin of quartz. *J. Sediment. Petrol.*, 57:373–377.

Clayton, R. N., and Mayeda, T. K., 1963. The use of bromide pentafluoride in the extraction of oxygen from oxides and silicates for isotopic analysis. *Geochim. Cosmochim. Acta*, 27:43–52.

Clayton, R. N., O'Neil, J. R., and Mayeda, T. K., 1972. Oxygen isotope exchange between quartz and water. *J. Geophys. Res.*, 77:3057–3067.

Coates, A. G., 1973. Cretaceous Tethyan coral-rudist biogeography related to the evolution of the Atlantic Ocean. *In Organisms and Continents through Time*: Paleontol. Assoc. London Spec. Pap. Paleontol., 12:169–174.

Dapples, E. C., 1962. Stages of diagenesis in the development of sandstones. *Geol. Soc. Am. Bull.*, 73:913–933.

Deines, P., and Gold, D. P., 1969. The change in carbon and oxygen isotopic composition during contact metamorphism of Trenton limestone by the Mount Royal pluton. *Geochim. Cosmochim. Acta*, 37: 1709–1733.

Dravis, J. J., and Yurewicz, D. A., 1985. Enhanced carbonate petrography using fluorescence microscopy. *J. Sediment. Petrol.*, 55:795–804.

Faure, G., 1977. *Principles of Isotope Geology*: Santa Barbara, CA (Wiley).

Haggerty, J. A., 1987. Petrology, and carbon and oxygen stable isotopic composition of macrofossils and sediments from the Blake-Bahama Formation, Deep Sea Drilling Program Site 603, western North Atlantic lower continental rise. *In* van Hinte, J. E., Wise, S. W., Jr., et al., *Init. Repts. DSDP*, 93: Washington (U.S. Govt. Printing Office), 1003–1021.

Hallock, P., and Schlager, W., 1986. Nutrient excess and the demise of coral reefs and carbonate platforms. *Palaios*, 1:389–398.

Hower, J., Eslinger, E. V., Hower, M. E., and Perry, E. A., 1976. The mechanism of burial metamorphism of argillaceous sediments: 1. Mineralogical and chemical evidence. *Geol. Soc. Am. Bull.*, 87:725–737.

Jansa, L. F., Enos, P., Tucholke, B. E., Gradstein, F. M., and Sherdian, R. E., 1979. Mesozoic-Cenozoic sedimentary formations of the North American Basin; western North Atlantic. *In* Talwani, M., Hay, W., and Ryan, W.B.F. (Eds.), *Deep Drilling Results in the Atlantic Ocean: Continental Margins and Paleoenvironment*: Am. Geophys. Union, Maurice Ewing Ser., 3:1–57.

Knauth, L. P., and Epstein, S., 1976. Hydrogen and oxygen isotope ratios in silica from the JOIDES Deep Sea Drilling Project. *Earth Planet Sci. Lett.*, 25:1–10.

McClain, W. R., and Freeman-Lynde, R. P., 1987. Petrology and stable oxygen and carbon isotope composition of Campanian grainstones and rudstones, northeast Providence Channel, Bahamas: ODP Leg 101, Hole 634. *SEPM Ann. Midyear Meet. Abstr.*, 9:54. (Abstract)

McCrea, J. M., 1950. On the isotopic chemistry of carbonates and a paleotemperature scale. *J. Chem. Phys.*, 18:849–857.

Paulus, F. S., 1972. The geology of Site 98 and the Bahama Platform. *In* Hollister, C. D., Ewing, J. I. et al., *Init. Repts. DSDP*, 11: Washington (U.S. Govt. Printing Office), 877–897.

Perkins, B. F., 1974. Paleoecology of a rudist reef complex in the Comanche Cretaceous Glen Rose Limestone of central Texas. *Geosci. Man*, 8:131–173.

Prezbindowski, D. R., and Pittman, E. D., 1987. Petrology and geochemistry of sandstones in the Lower Cretaceous submarine fan complex, DSDP Hole 603B. *In* van Hinte, J. E., Wise, S. W., Jr., et al., *Init. Repts. DSDP*, 93: Washington (U.S. Govt. Printing Office), 961–976.

Robertson, A.H.F., and Bliefnick, D. M., 1983. Sedimentology and origin of Lower Cretaceous pelagic carbonates and redeposited clastics, Blake-Bahama Formation, Deep Sea Drilling Project Site 534, western equatorial Atlantic. *In* Sheridan R. E., Gradstein, F. M., et al., *Init. Repts. DSDP*, 76: Washington (U.S. Govt. Printing Office), 795–827.

Roedder, E., 1984. *Fluid Inclusions*: Rev. Mineral., 12.

Schlager, W., 1980. Mesozoic calciturbidites in Deep Sea Drilling Project Hole 416A: recognition of a drowned carbonate platform. *In* Lancelot, Y., Winterer, E. L., et al., *Init. Repts. DSDP*, 50: Washington (U.S. Govt. Printing Office), 733–749.

Schlager, W., and Ginsburg, R. N., 1981. Bahama carbonate platforms—the deep and the past. *Mar. Geol.*, 44:1–24.

Shackleton, N. J., and Kennett, J. P., 1975. Paleotemperature history of the Cenozoic and the initiation of Antarctic glaciation: oxygen and carbon isotope analyses in DSDP Sites 277, 279, and 281. *In* Kennett, J. P., Houtz, R. E., et al., *Init. Repts. DSDP*, 29: Washington (U.S. Govt. Printing Office), 743–755.

Shepard, T., Rankin, A. H., and Alderton, D.H.M., 1985. *A Practical Guide to Fluid Inclusion Studies*: New York (Chapman and Hall).

Shipboard Scientific Party, 1987a. Site 683. *In* Boillot, G., Winterer, E. L., et al., *Proc. ODP, Init. Repts.*, 103: College Station, TX (Ocean Drilling Program), 221–407.

_____, 1987b. Site 641. *In* Boillot, G., Winterer, E. L., et al., *Proc. ODP, Init. Repts.*, 103: College Station, TX (Ocean Drilling Program), 571–649.

Smith, J. V., and Stenstrom, R. C., 1966. Electron-excited luminescence as a petrologic tool. *J. Geol.*, 73:627–635.

Smith, M. P., 1986. Silver coating inhibits electron microprobe beam damage of carbonates. *J. Sediment. Petrol.*, 56:560–561

Vail, P. R., Mitchum, R. M., Jr., Todd, R. G., Widmier, J. M., Thompson, S., III, Sangree, J. B., Bubb, J. N., and Hatlelid, W. G., 1977. Seismic stratigraphy and global changes of sea level. *In* Payton, C. E. (Ed.), *Application to Hydrocarbon Exploration*: Mem. Am. Assoc. Pet. Geol., 26:49–212.

van Gijzel, P., 1979. *Manual of the Techniques and Some Geological Applications of Fluorescence Microscopy*: Dallas (Am. Assoc. Stratigr. Palynol.).

Date of initial receipt: 6 April 1987
Date of acceptance: 17 December 1987
Ms 103B-128